Lifetime measurements in ^{53}Ca

S. Chen
on behalf of the HiCARI collaboration
and the RIBF-170 collaboration

University of York

Liverpool, 10th April 2024

Shell structures and nuclear forces

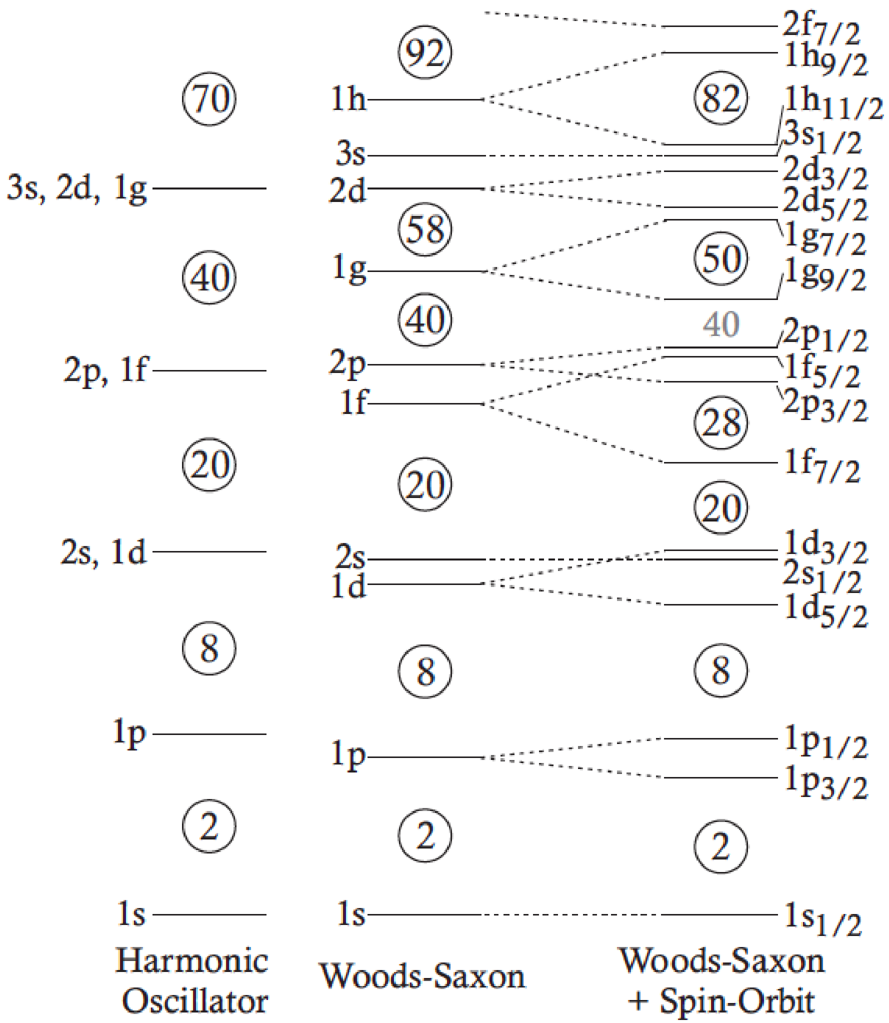

Maria Goeppert-Mayer
& Hans D. Jensen
1963

Maria Goeppert-Mayer, Phys. Rev. **75**, 1969 (1949)
O. Haxel, Phys. Rev. **75**, 1766 (1949)

Shell structures and nuclear forces

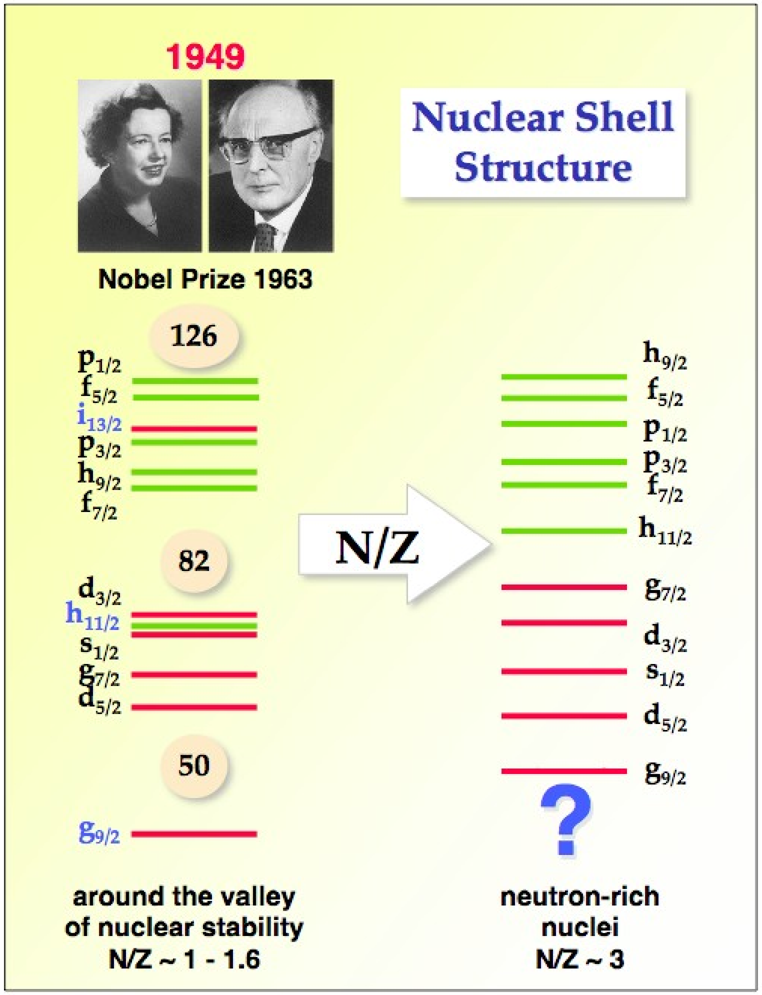

- Shell structure and magic numbers were the cornerstones of the shell model for many decades
- Experiments on exotic nuclei found magic numbers are not immutable throughout the nuclear chart
- Shell structure is now recognized as local concept

J. Dobaczewski *et al.*, Prog. Part. Nucl. Phys. **59** (2007) 432–445

Shell structures and nuclear forces

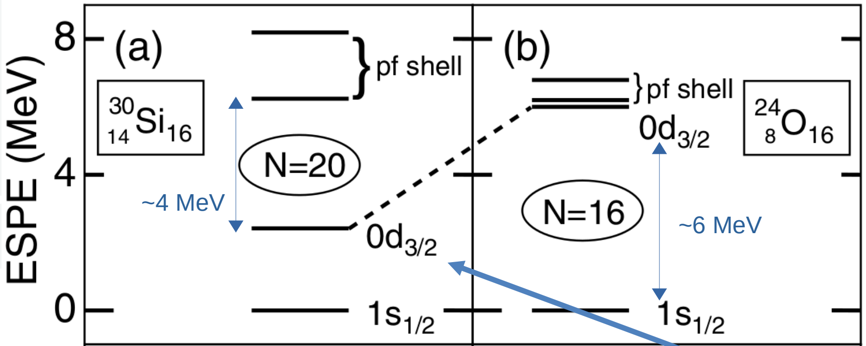

T. Otsuka *et al.*, Phys. Rev. Lett. **87**, 082502 (2001)

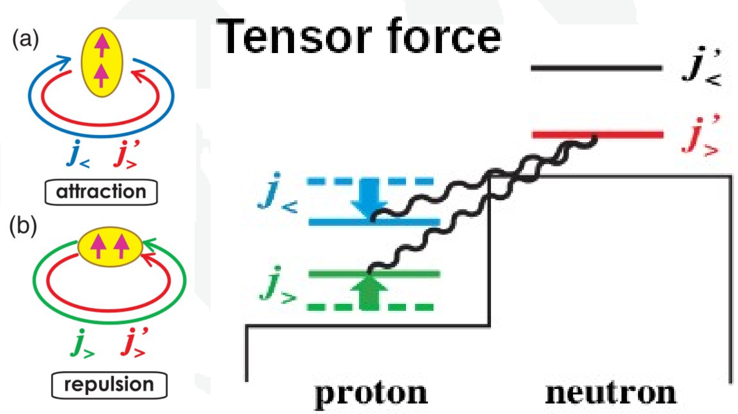

T. Otsuka *et al.*, Phys. Rev. Lett. **95**, 232502 (2005)

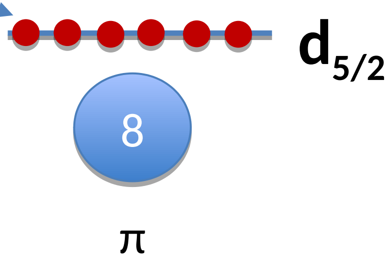

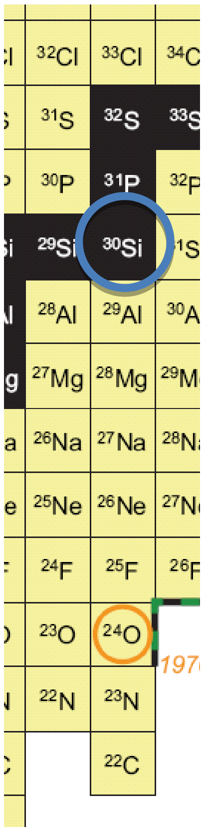

Tensor force: attractive when the intrinsic spins of neutron and proton are anti-parallel and repulsive when they are parallel

$^{30}Si \rightarrow ^{24}O$: absence of strong $\pi 0d_{5/2} - \nu 0d_{3/2}$ attraction

$\Rightarrow$ N = 16 new magic number in oxygen

Shell structures and nuclear forces

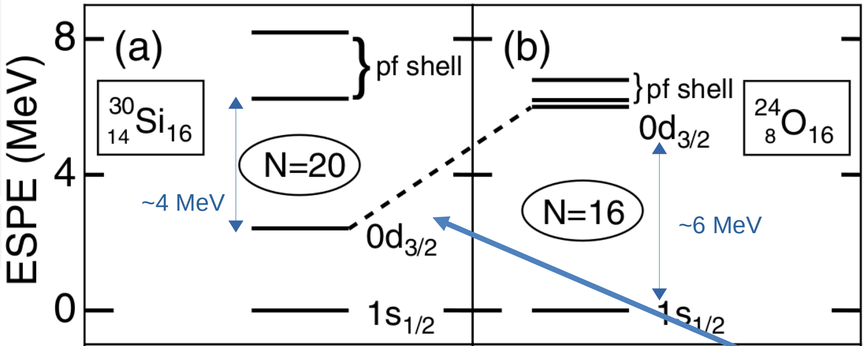

T. Otsuka *et al.*, Phys. Rev. Lett. **87**, 082502 (2001)

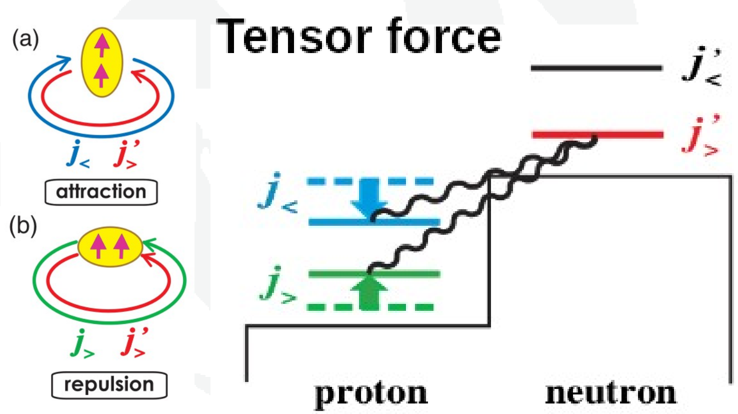

T. Otsuka *et al.*, Phys. Rev. Lett. **95**, 232502 (2005)

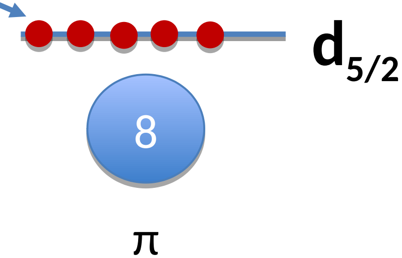

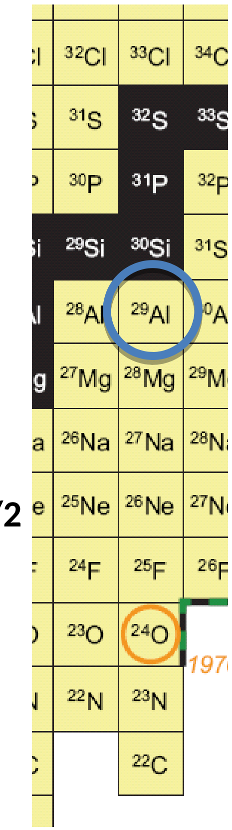

Tensor force: attractive when the intrinsic spins of neutron and proton are anti-parallel and repulsive when they are parallel

$^{30}Si \rightarrow {}^{24}O$: absence of strong $\pi 0d_{5/2} - \nu 0d_{3/2}$ attraction

$\Rightarrow$ $N = 16$ new magic number in oxygen

Shell structures and nuclear forces

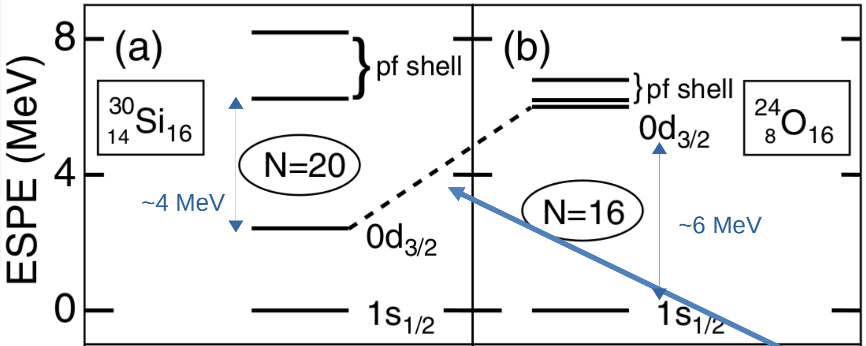

T. Otsuka *et al.*, Phys. Rev. Lett. **87**, 082502 (2001)

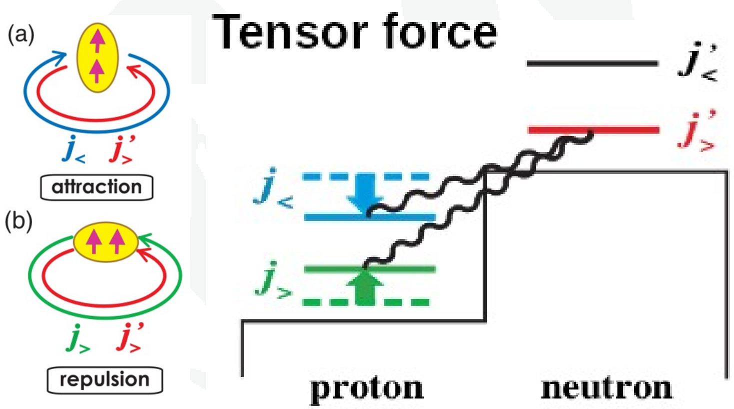

T. Otsuka *et al.*, Phys. Rev. Lett. **95**, 232502 (2005)

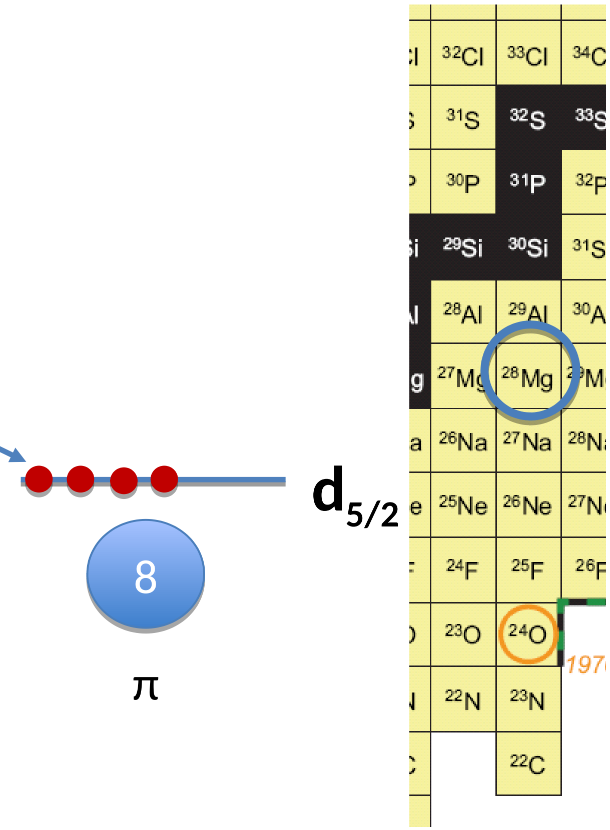

^{30}Si → ^{24}O: absence of strong $\pi 0d_{5/2} - \nu 0d_{3/2}$ attraction

⇒ N = 16 new magic number in oxygen

Tensor force: attractive when the intrinsic spins of neutron and proton are anti-parallel and repulsive when they are parallel

Shell structures and nuclear forces

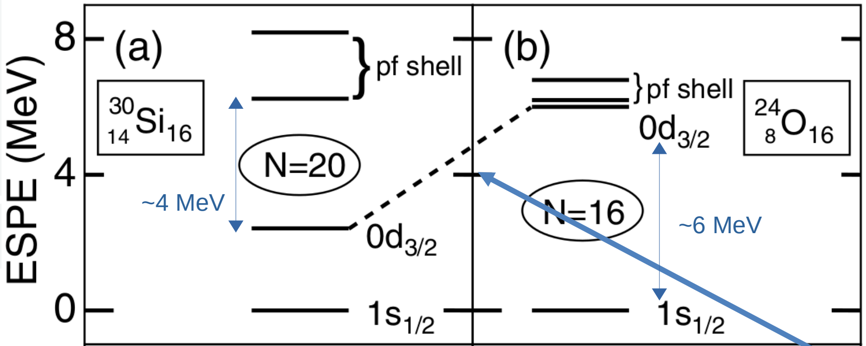

T. Otsuka *et al.*, Phys. Rev. Lett. **87**, 082502 (2001)

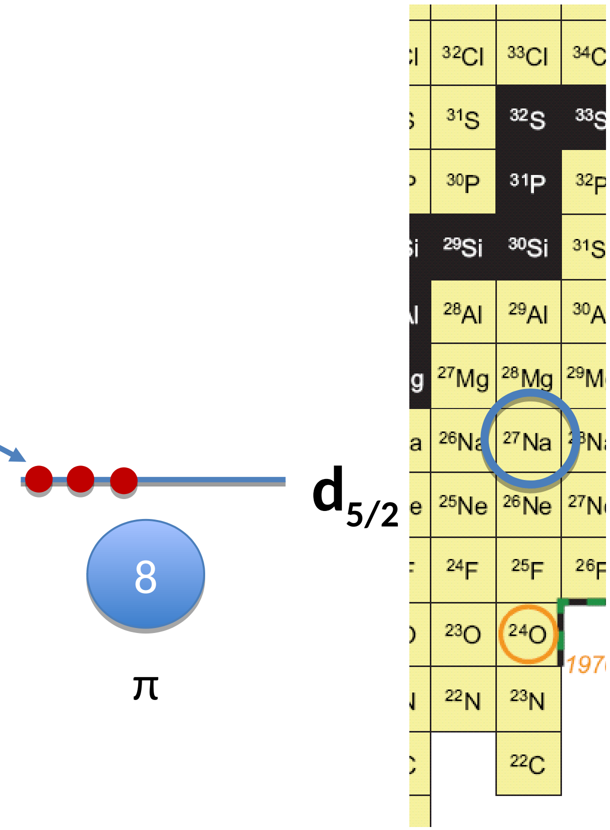

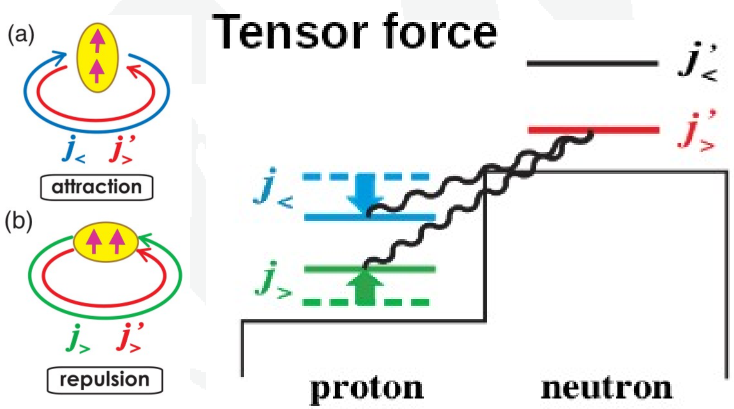

T. Otsuka *et al.*, Phys. Rev. Lett. **95**, 232502 (2005)

$^{30}Si \rightarrow {}^{24}O$: absence of strong $\pi 0d_{5/2} - \nu 0d_{3/2}$ attraction

$\Rightarrow$ $N = 16$ new magic number in oxygen

Tensor force: attractive when the intrinsic spins of neutron and proton are anti-parallel and repulsive when they are parallel

Shell structures and nuclear forces

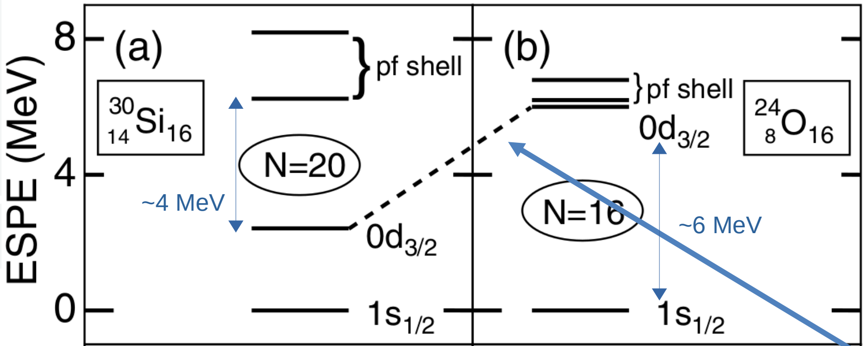

T. Otsuka *et al.*, Phys. Rev. Lett. **87**, 082502 (2001)

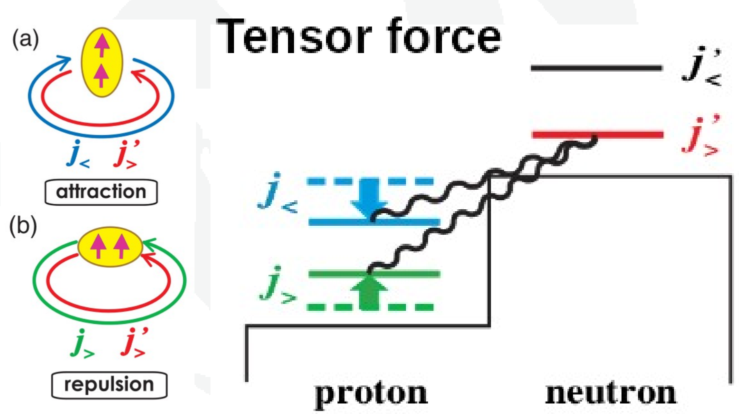

T. Otsuka *et al.*, Phys. Rev. Lett. **95**, 232502 (2005)

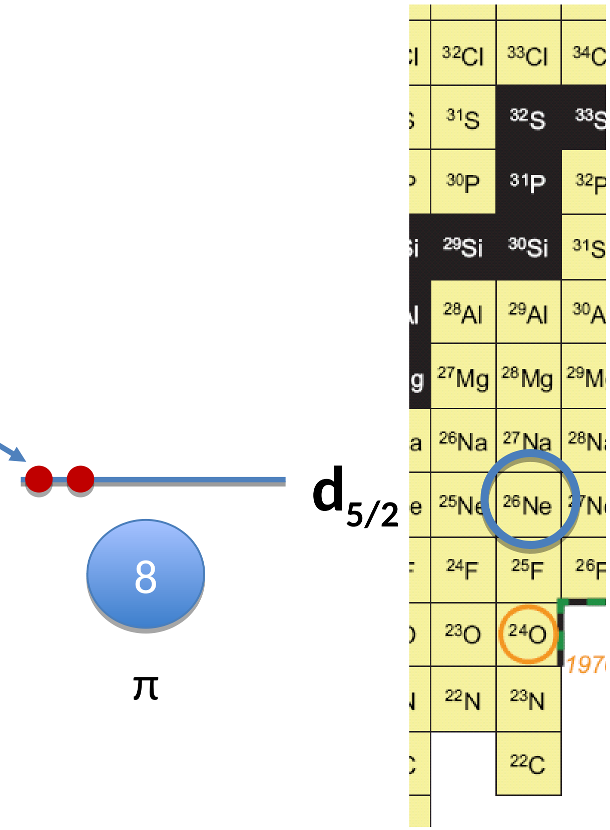

Tensor force: attractive when the intrinsic spins of neutron and proton are anti-parallel and repulsive when they are parallel

$^{30}Si \rightarrow {}^{24}O$: absence of strong $\pi 0d_{5/2} - \nu 0d_{3/2}$ attraction

$\Rightarrow$ $N = 16$ new magic number in oxygen

Shell structures and nuclear forces

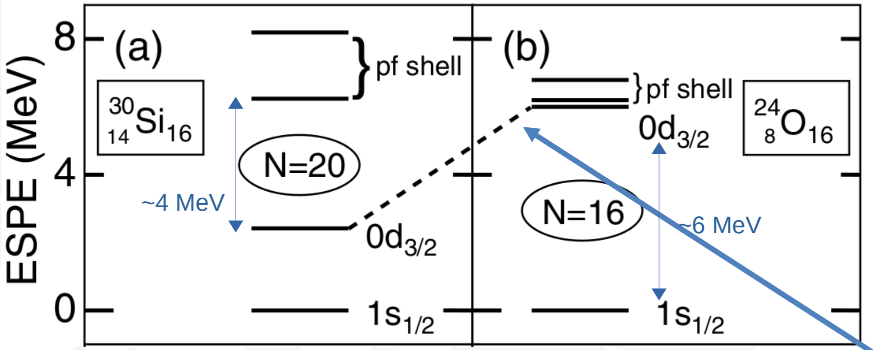

T. Otsuka *et al.*, Phys. Rev. Lett. **87**, 082502 (2001)

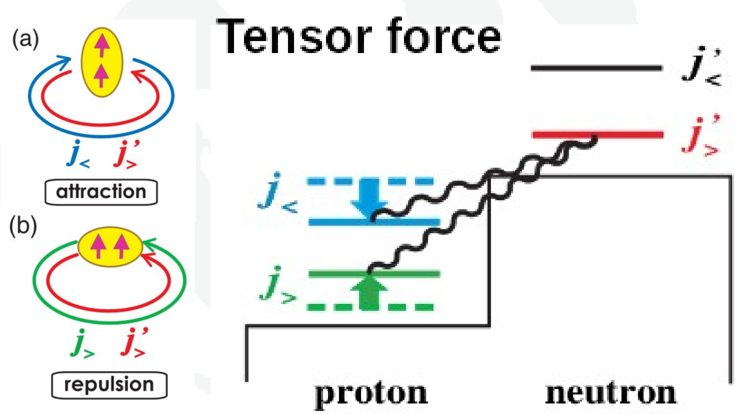

T. Otsuka *et al.*, Phys. Rev. Lett. **95**, 232502 (2005)

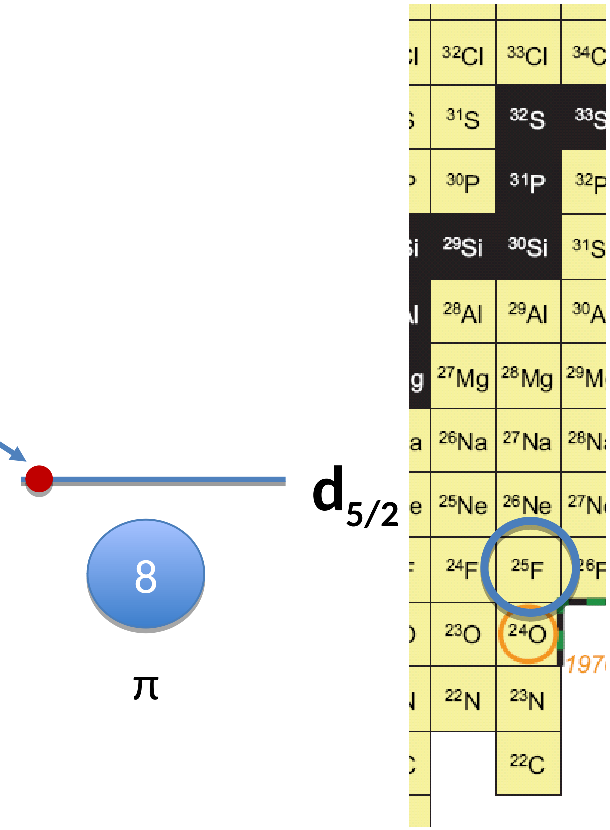

Tensor force: attractive when the intrinsic spins of neutron and proton are anti-parallel and repulsive when they are parallel

^{30}Si → ^{24}O: absence of strong $\pi 0d_{5/2} - \nu 0d_{3/2}$ attraction

⇒ N = 16 new magic number in oxygen

Shell structures and nuclear forces

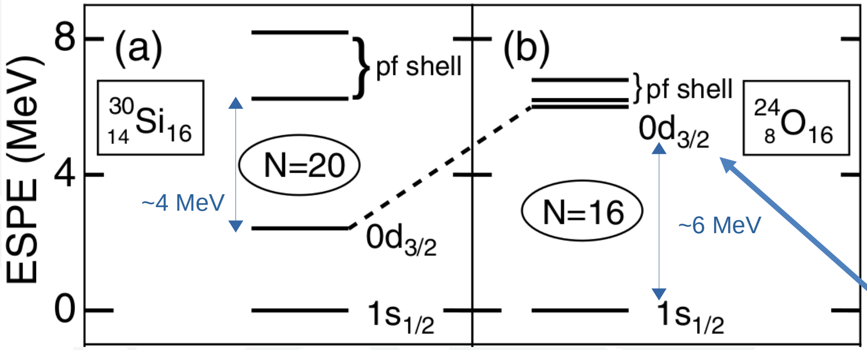

T. Otsuka *et al.*, Phys. Rev. Lett. **87**, 082502 (2001)

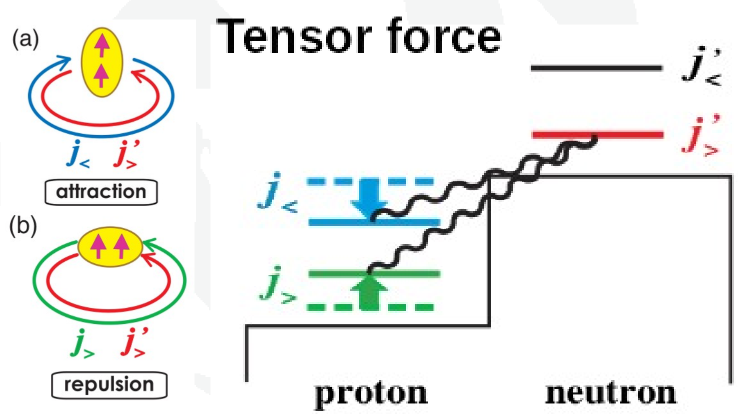

T. Otsuka *et al.*, Phys. Rev. Lett. **95**, 232502 (2005)

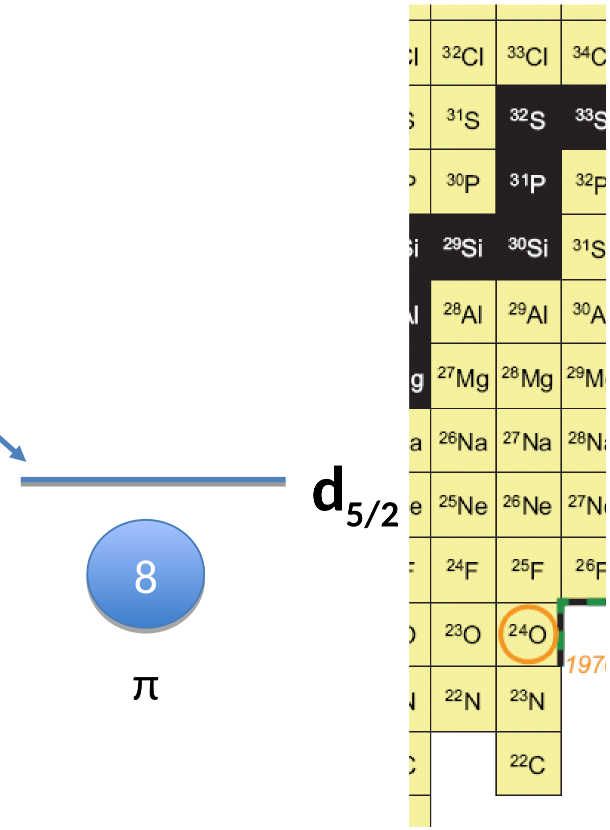

Tensor force: attractive when the intrinsic spins of neutron and proton are anti-parallel and repulsive when they are parallel

^{30}Si → ^{24}O: absence of strong $\pi 0d_{5/2} - \nu 0d_{3/2}$ attraction

⇒ $N = 16$ new magic number in oxygen

N = 32,34 shell closure in Ca isotopes

D. Steppenbeck *et al.*, Nature **502**,207-10 (2013)

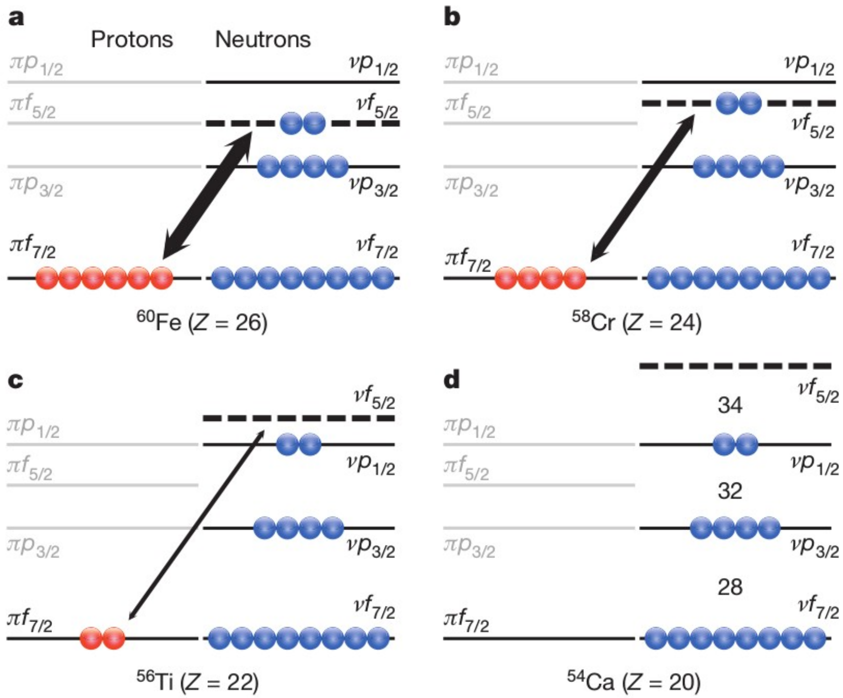

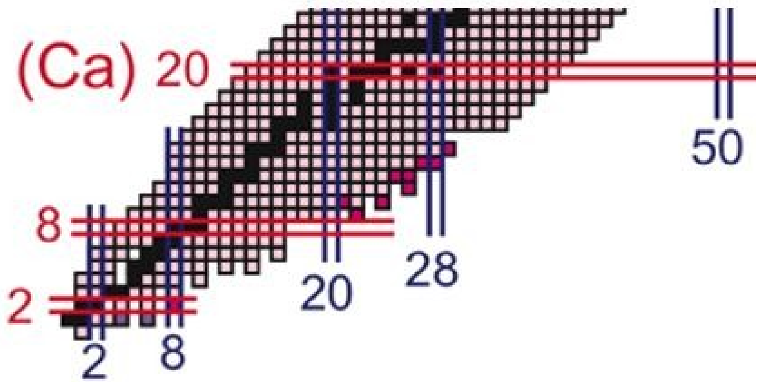

(sub-)shell closure at N = 16, 20, 28, 32, 34

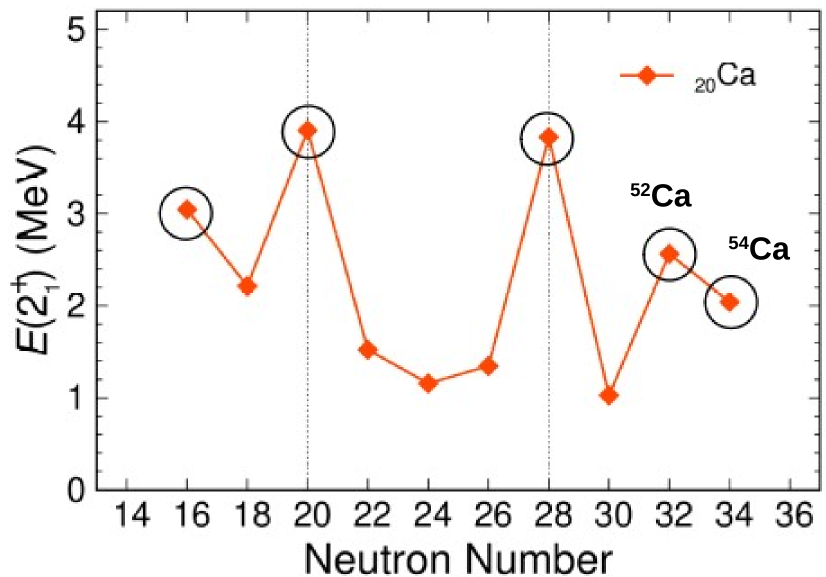

- Absence of strong $\pi f_{7/2} - \nu f_{5/2}$ attraction make N = 32,34 new magic number in calcium

N = 32 shell closure in ^{52}Ca

D. Steppenbeck *et al.*, Nature **502**,207-10 (2013)

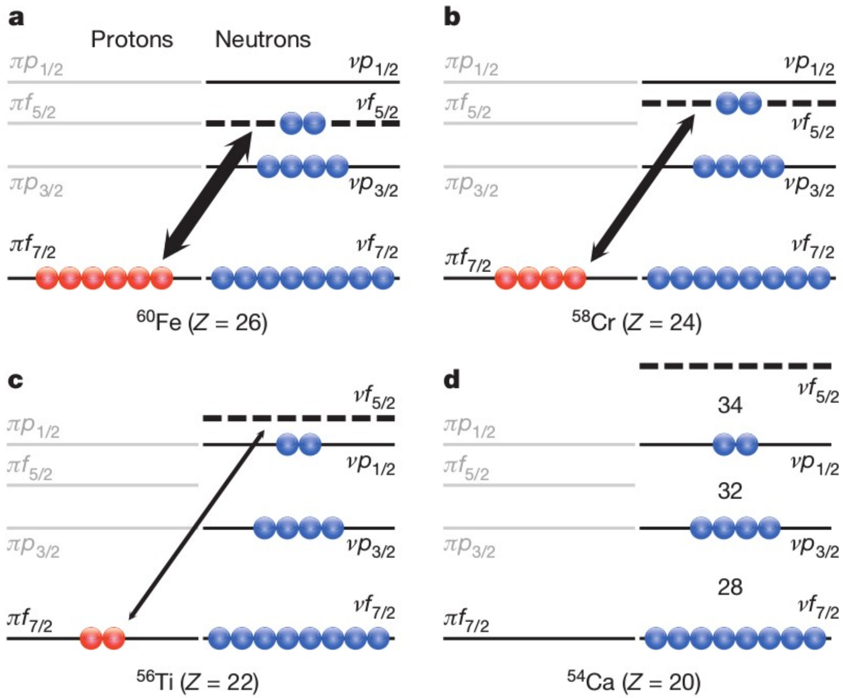

A. Huck *et al.*, Phys. Rev. C **31**,2226-2237 (1985)

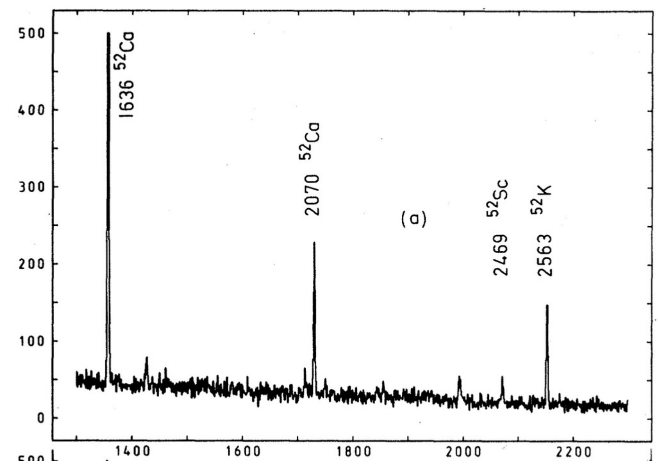

F. Wienholtz *et al.*, Nature **498**, 346-349 (2013)

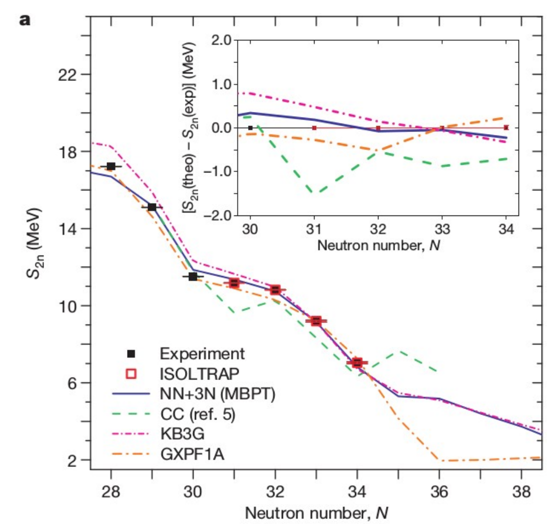

- Absence of strong $\pi f_{7/2} - \nu f_{5/2}$ attraction make N = 32,34 new magic number in calcium
- Experimental evidences for ***N* = 32** magic
  - Large E(2^+_1)
  - Mass measurement: large empirical two-neutron shell gap

N = 34 shell closure in ^{54}Ca

D. Steppenbeck *et al.*, Nature **502**,207-10 (2013)

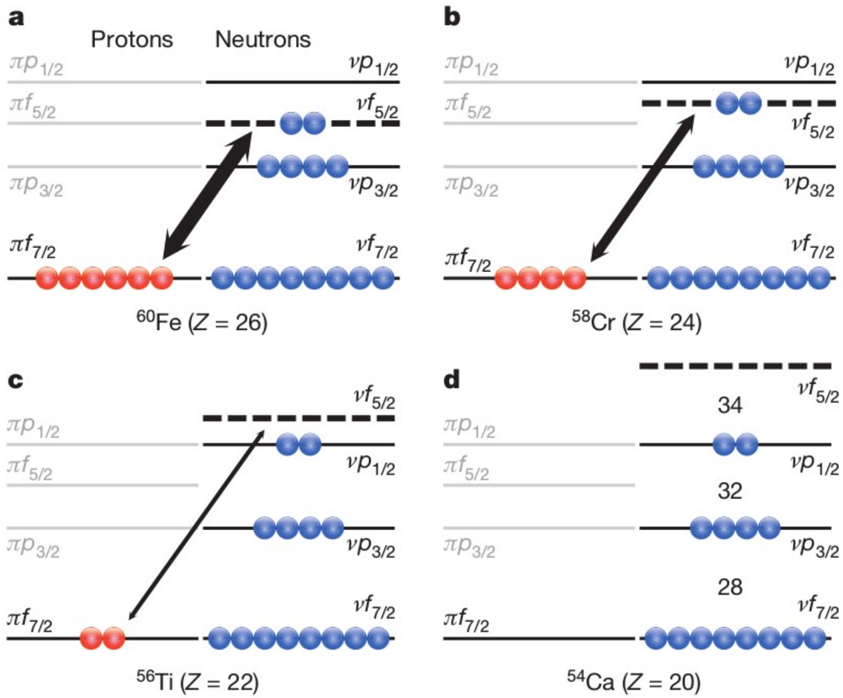

D. Steppenbeck *et al.*, Nature **502**,207-10 (2013)

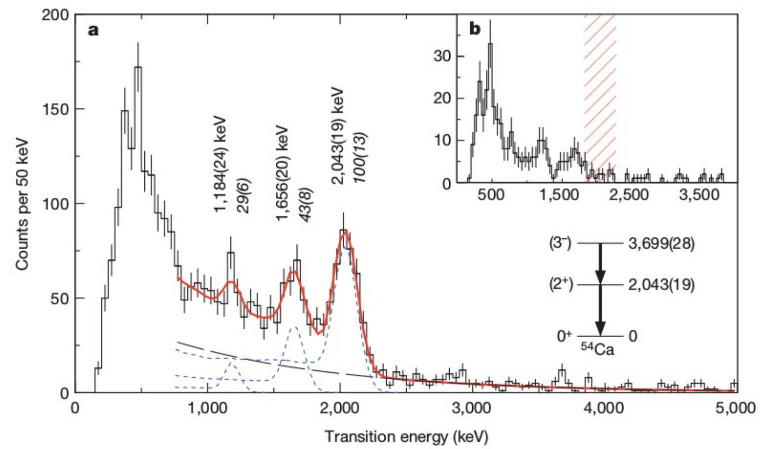

S. Michimasa *et al.*, Phys. Rev. Lett. **121**, 022506 (2018)

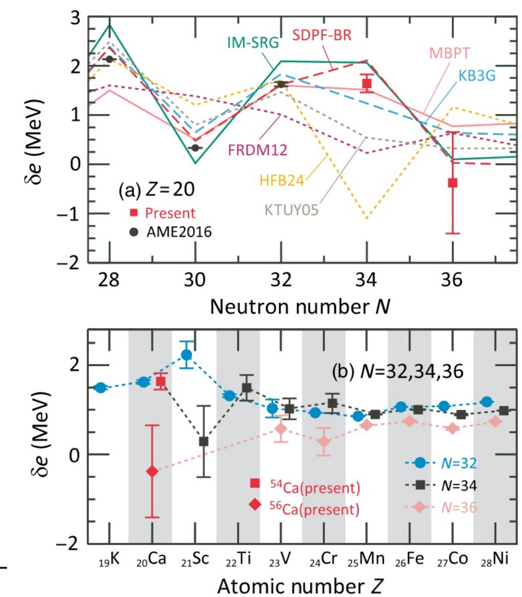

- Absence of strong $\pi f_{7/2} - \nu f_{5/2}$ attraction make N = 32,34 new magic number in calcium
- Experimental evidences for ***N* = 34** magic
  - E(2^+_1): first evidence of magicity
  - Mass measurement: N = 34 shell gap similar size with N = 32 shell gap

Excitation of ^{53}Ca

D. Steppenbeck *et al.*, Nature **502**,207-10 (2013)

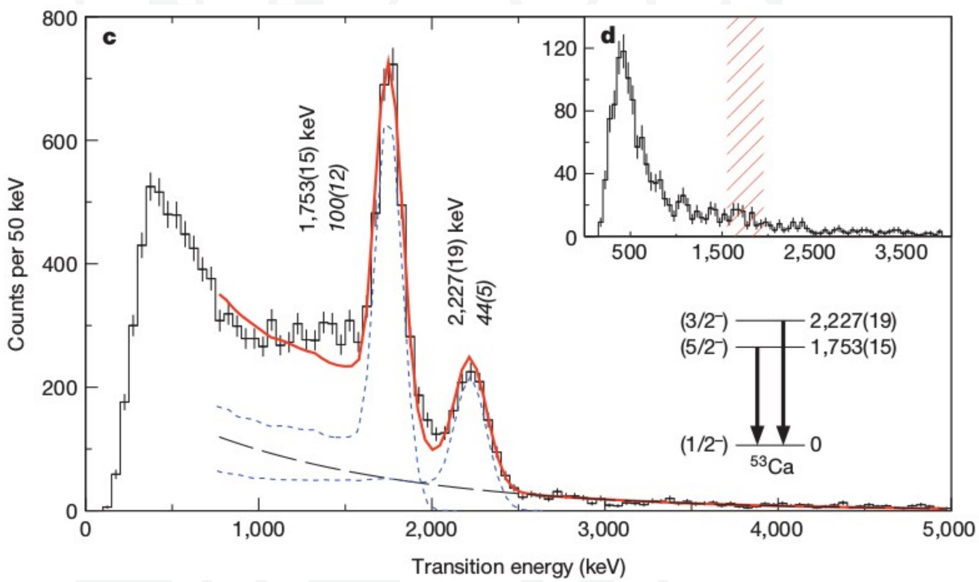

E_x = 2220 keV via β-decay,
F. Perrot *et al.* PRC **74**,014313 (2006)

S. Chen *et al.*, PRL **123**,142501 (2019)

State	Energy (keV)	GXPF1Bs	NNLOsat	*NN*+3*N* (lnl)
3/2-	2220(13)	2061	2635	2611
5/2-	1738(17)	1934	1950	2590

Lifetime measurements:

- E2 transition probability
- Benchmarks to test different theoretical descriptions beyond excitation energies

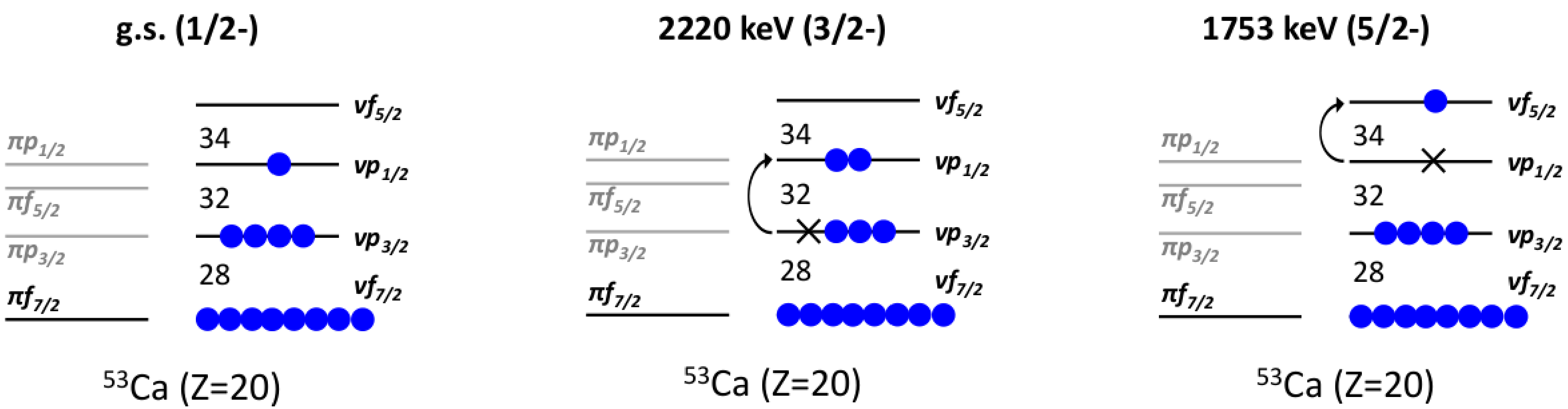

Lifetime measurement method

- Detect prompt gamma rays from fast moving (~0.5c) particles
- Doppler correction for prompt gamma

$$E_{\gamma 0} = E_{\gamma} \frac{1 - \beta \cos\theta}{\sqrt{1 - \beta^2}}$$

- Finite excitation state lifetime lead to θ and β distribution different from zero lifetime

  ==> asymmetric peak shape after Doppler-correction

- Peak shape analysis to extract excitation state lifetime

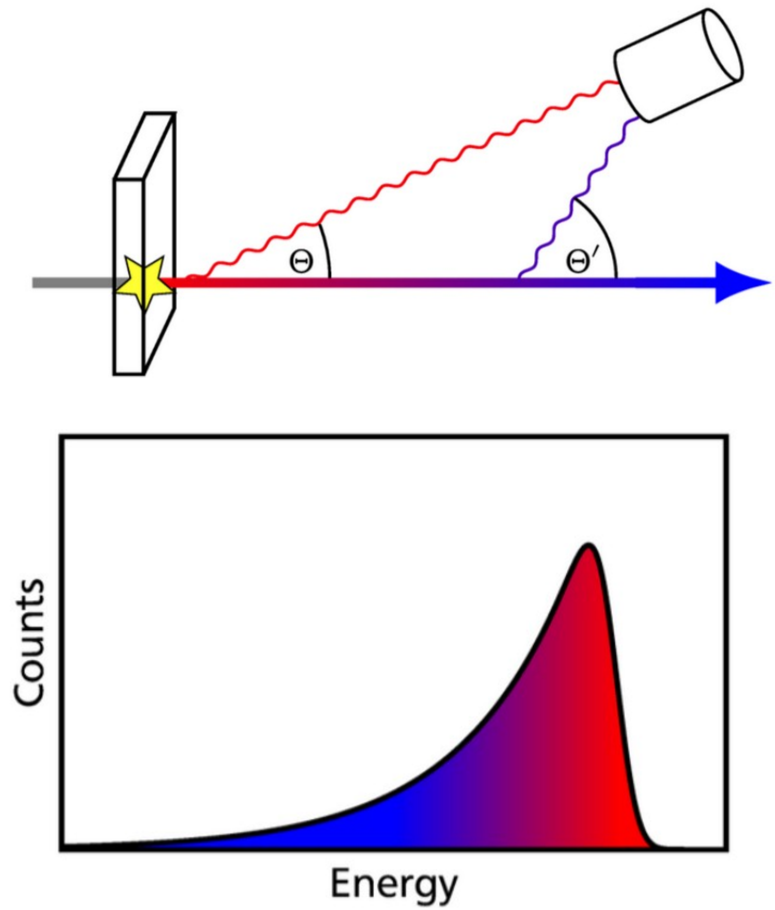

Figure: Schematic diagram of lifetime measurement method (Thesis, S. Heil, 2019)

Lifetime measurement method

- Detect prompt gamma rays from fast moving (~0.5c) particles
- Doppler correction for prompt gamma

$$E_{\gamma 0} = E_\gamma \frac{1 - \beta\cos\theta}{\sqrt{1-\beta^2}}$$

- Finite excitation state lifetime lead to θ and β distribution different from zero lifetime

  ==> asymmetric peak shape after Doppler-correction

- Peak shape analysis to extract excitation state lifetime

  ==> complicated lifetime responses, need compare with detailed simulations

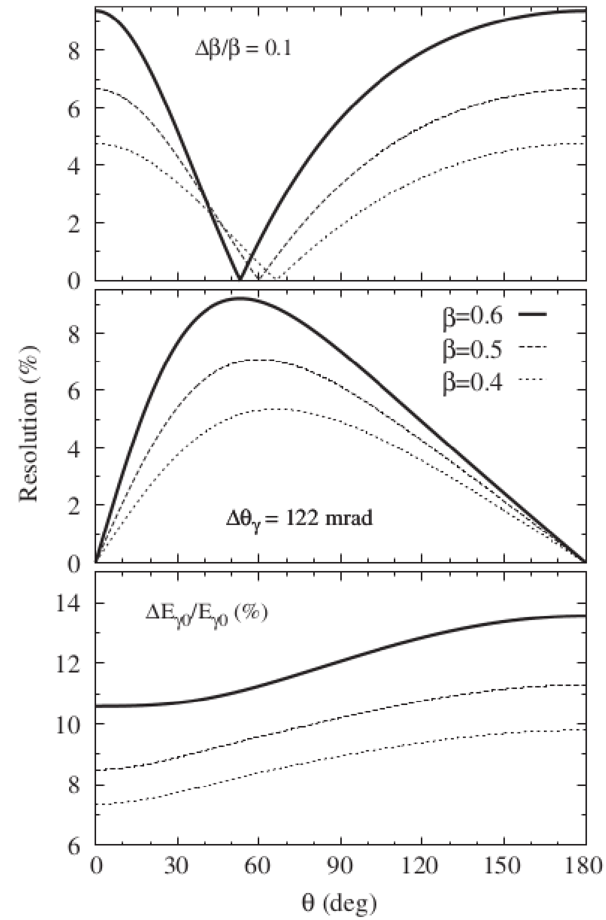

Figure: Doppler broadening as a function of gamma-emission angle (P. Doornenbal, PTEP **2012**, 03C004)

Experiment Setup at RIBF

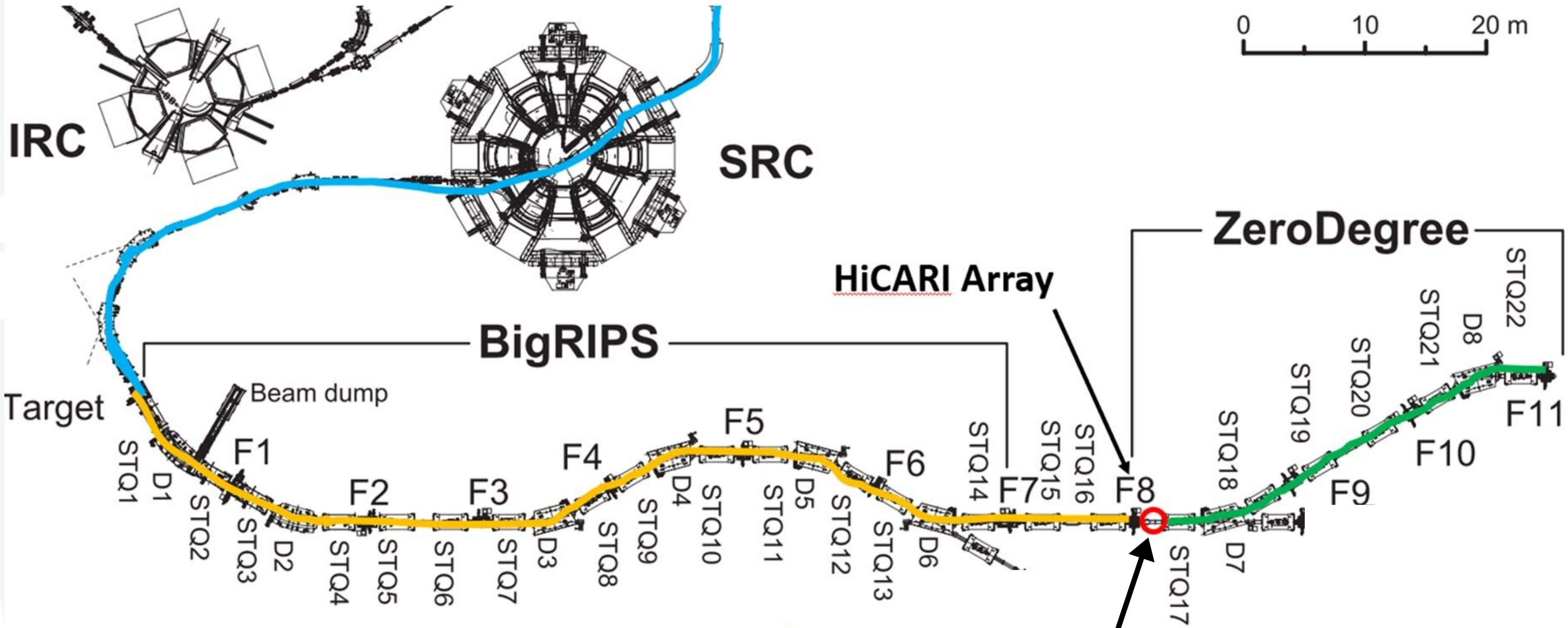

Beam Direction

Secondary targets

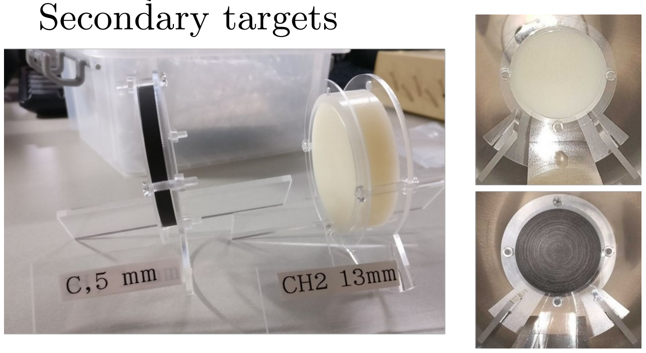

—	Primary Beam:	70 Zn Beam on Be target 354MeV/u
—	Secondary Beam:	Tuned to Sc isotopes
—	Tertiary Beam:	Tuned to Ca isotopes 220 MeV/u

Particle Identification

neutron-rich Ca setting

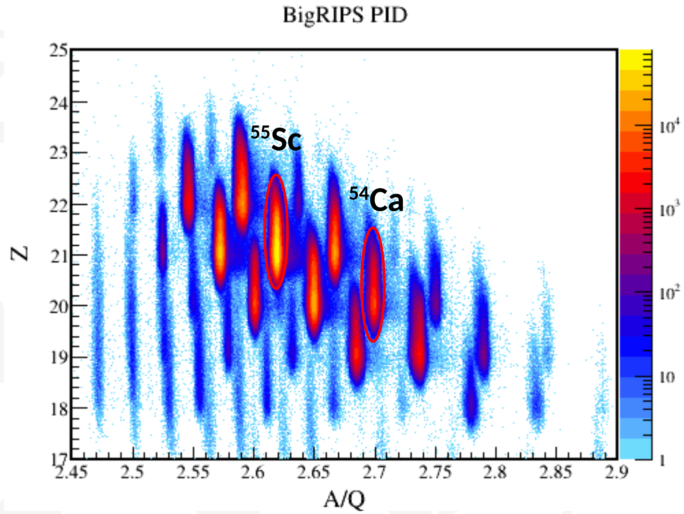

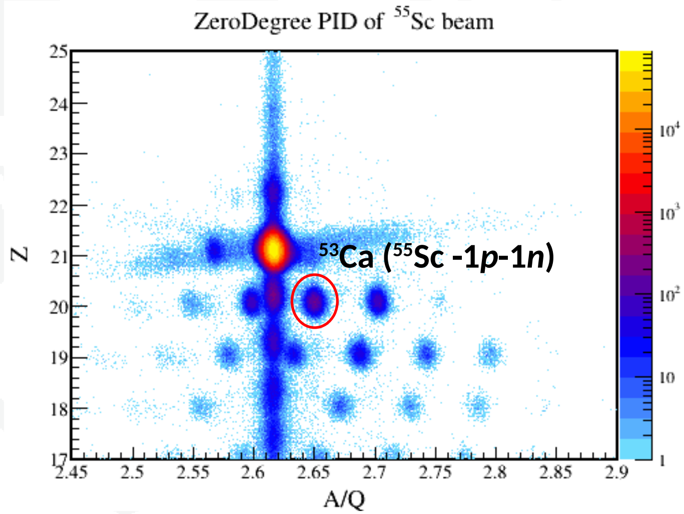

proton-rich Ca setting

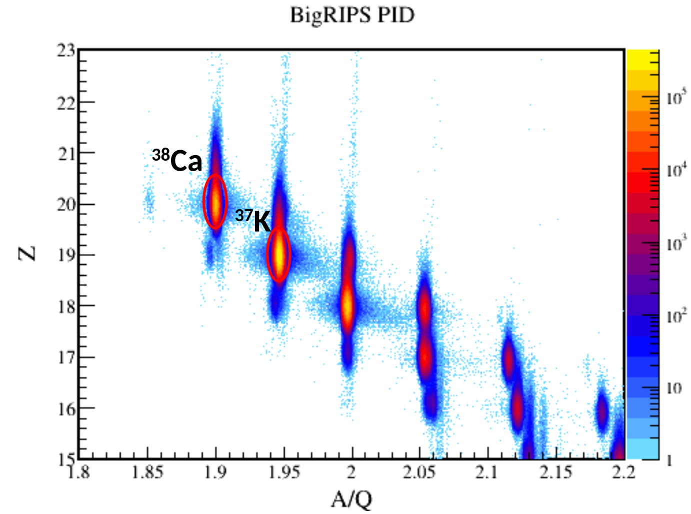

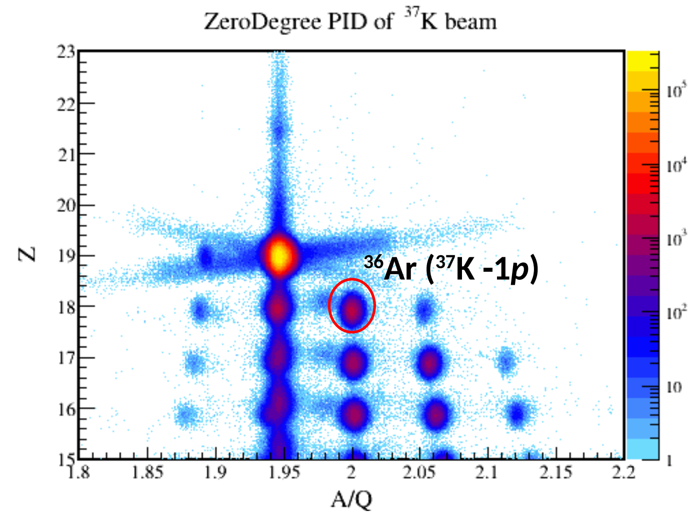

Experiment Setup – HiCARI

- **Hi**gh-resolution **C**luster **A**rray at the **RI**BF (RIKEN Accel. Prog., (2021), K. Wimmer, et. al.)
- Hybrid HPGe array:
  - 6 x Miniball cluster (6 segments)
  - 4 x SuperClover cluster (4 segments)
  - 1 x Gretina Quad cluster (position sensitive)
  - 1 x Gretina P3 cluster (position sensitive)

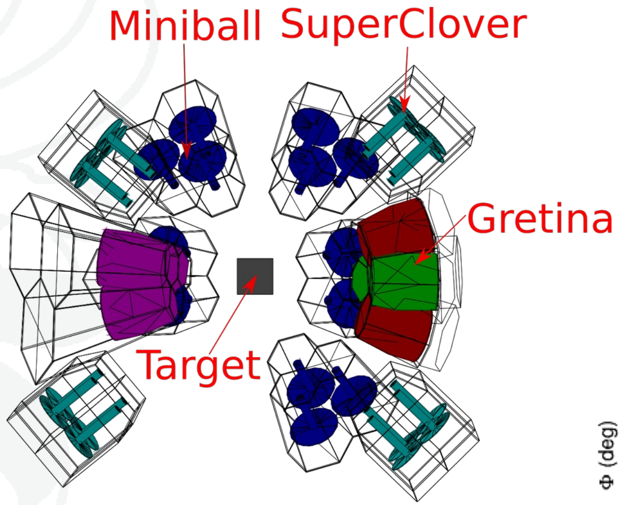

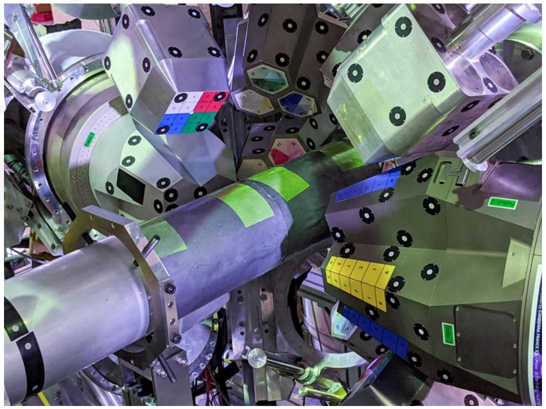

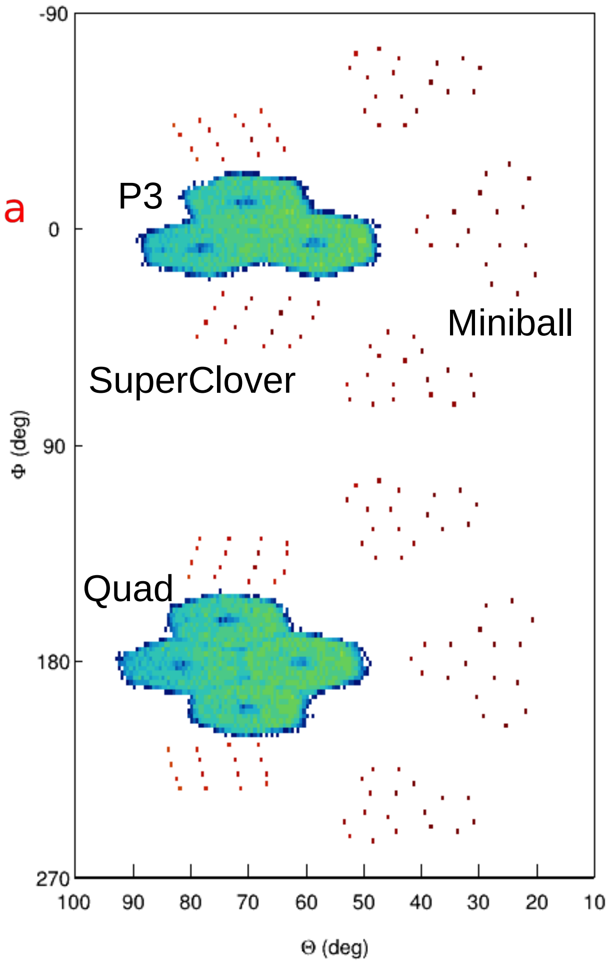

Figure: HiCARI array

Benchmark – ^{36}Ar from ^{37}K -1*p*

^{36}**Ar** low-lying excitation states from NNDC

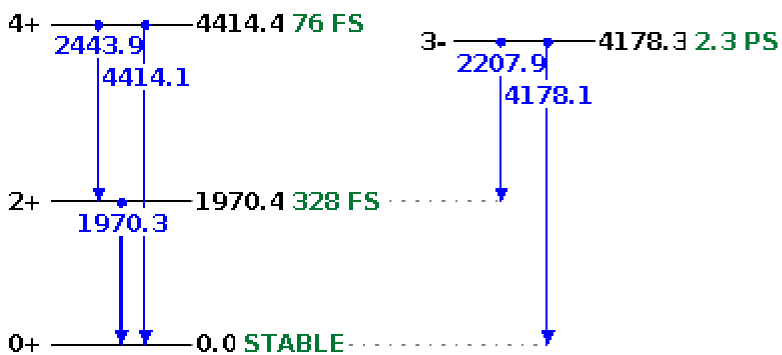

- Spectra of CH2 target have worse energy resolutions, due to large β uncertainty
- ^{36}Ar low-lying excitation states: known energy and lifetime

  ==> Benchmark Geant4 simulations

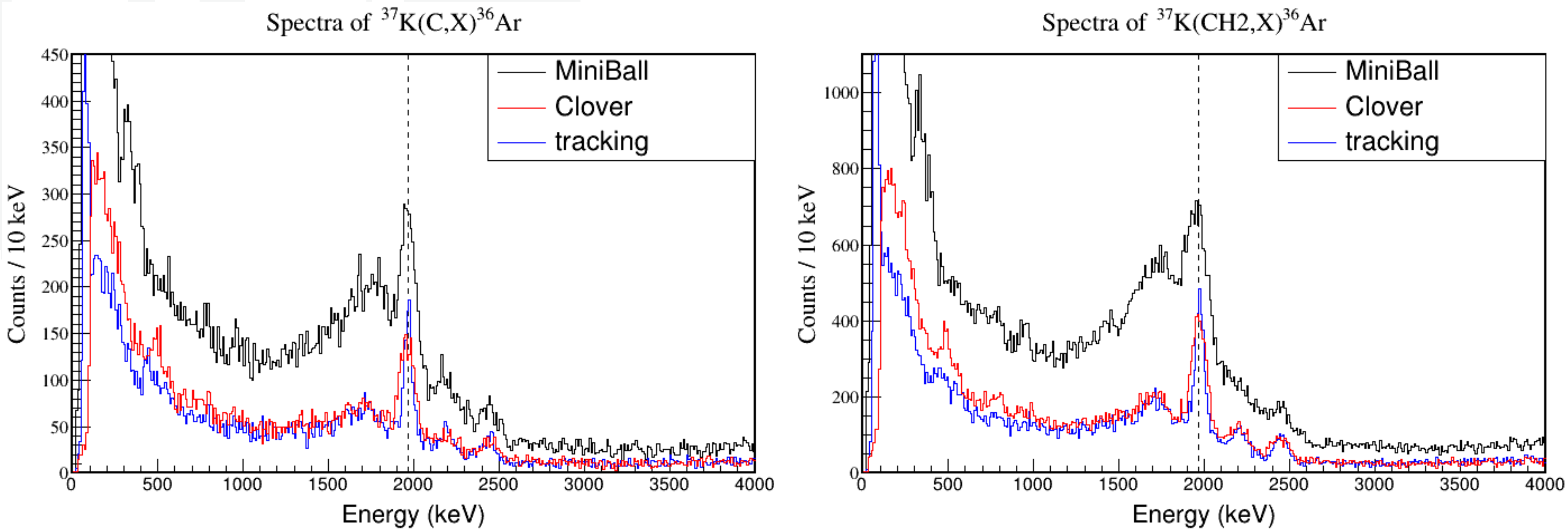

Figure: Doppler-corrected gamma-ray energy spectra

Benchmark – ^{36}Ar from ^{37}K -1*p*

^{36}**Ar** low-lying excitation states from NNDC

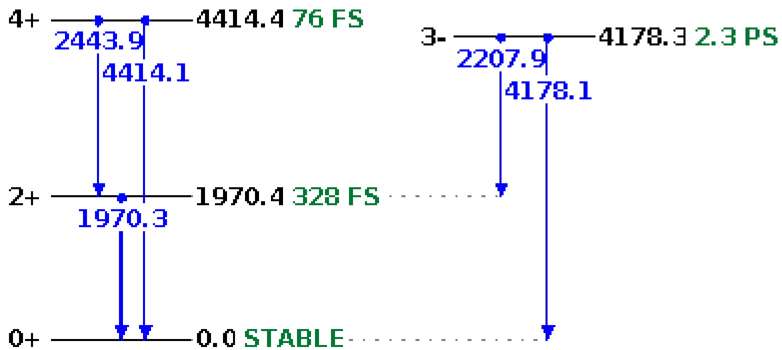

- Fitting function:
  Geant4 simulations + double-expo background

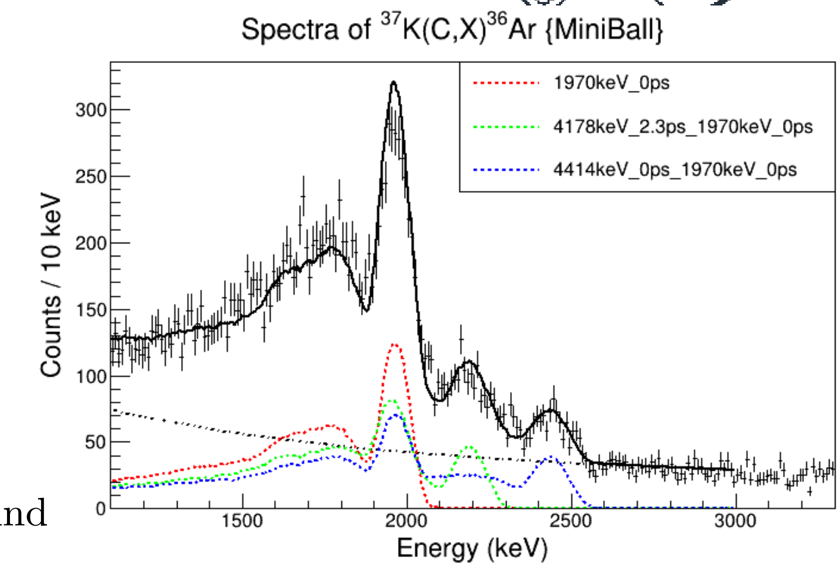

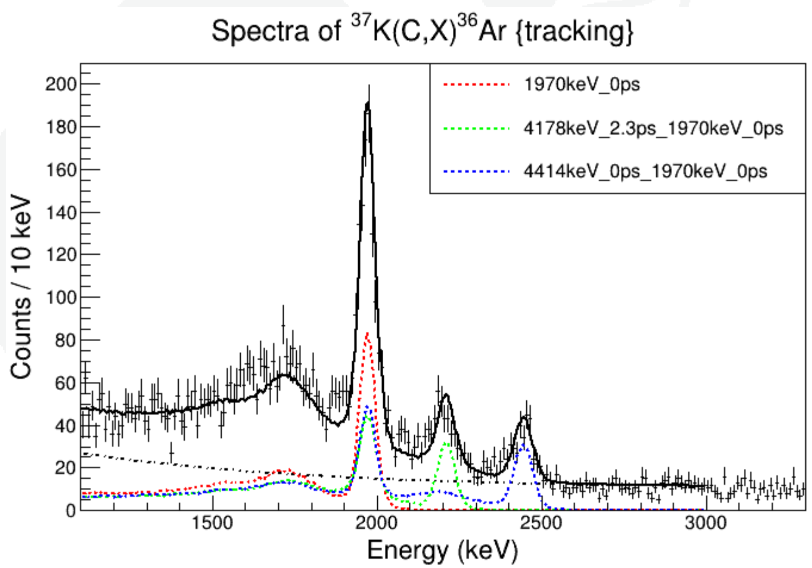

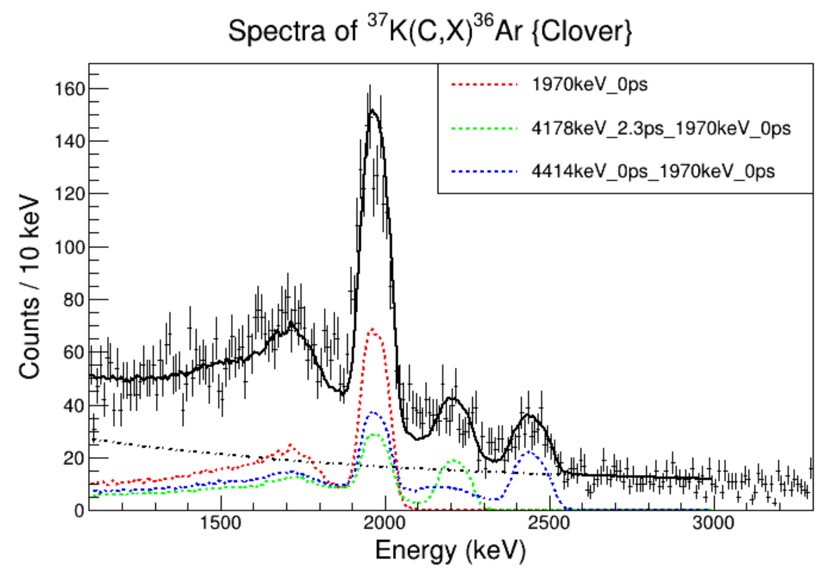

^{53}Ca from ^{55}Sc -1*p*1*n*

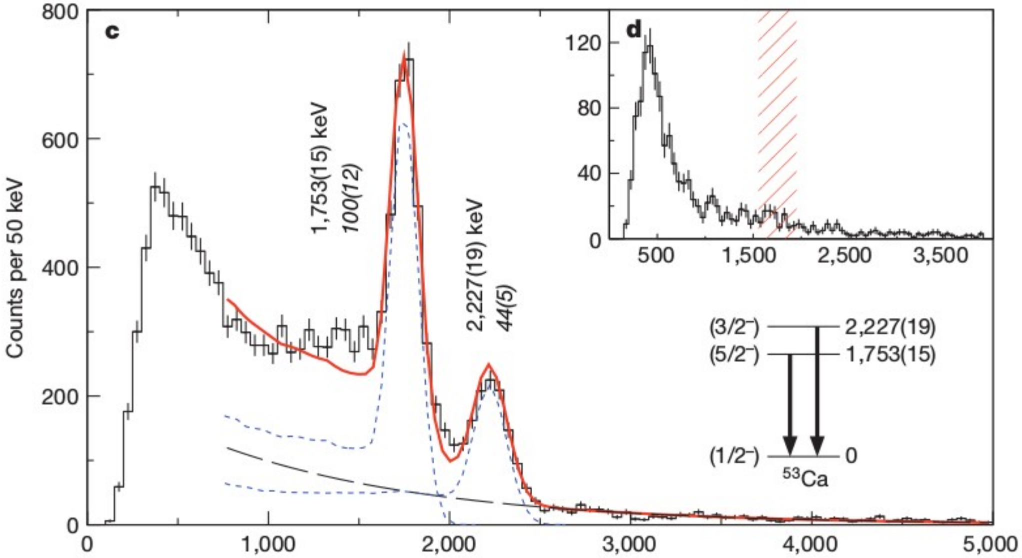

Previous measurement:

Gamma-ray spectra measured with NaI(Tl) detectors

D. Steppenbeck *et al.*, Nature **502**,207-10 (2013)

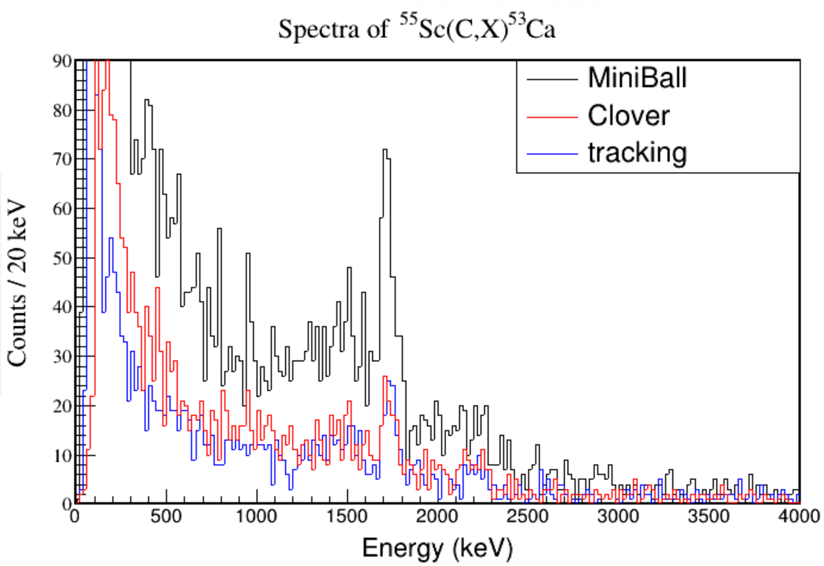

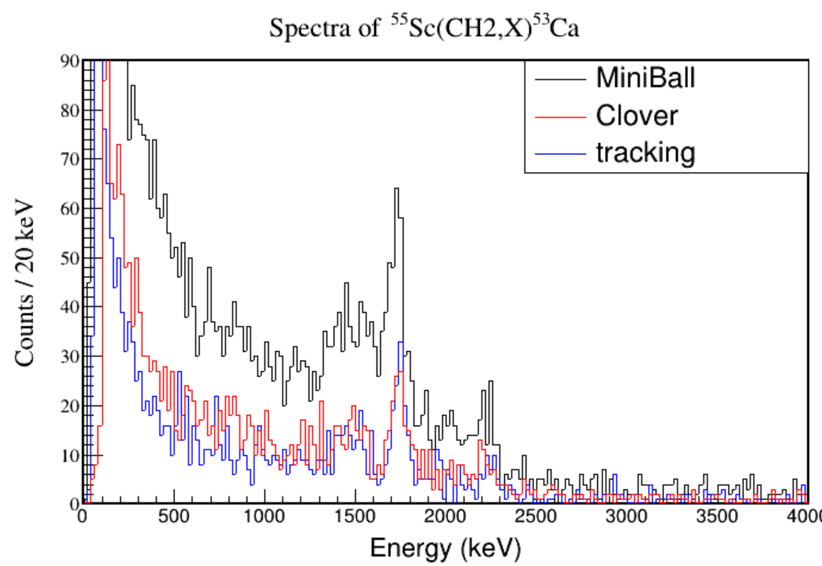

Figure: Doppler-corrected gamma-ray energy spectra

^{53}Ca from ^{55}Sc -1p1n

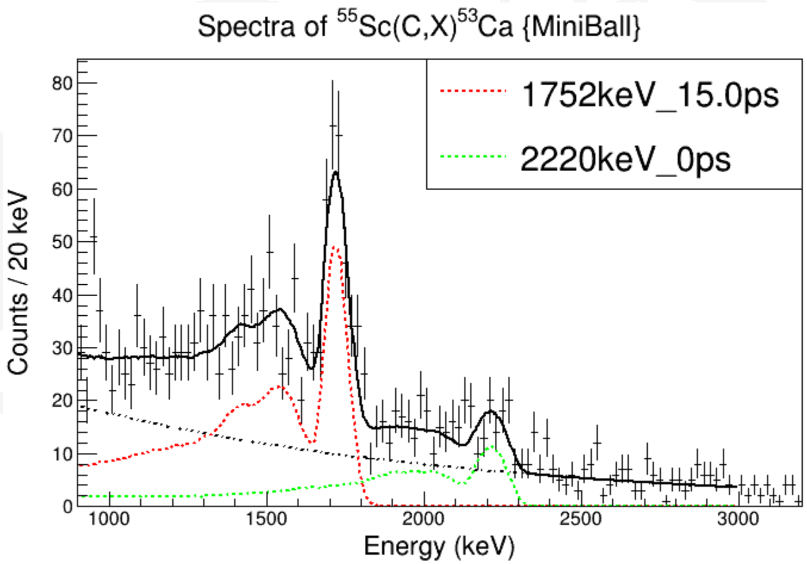

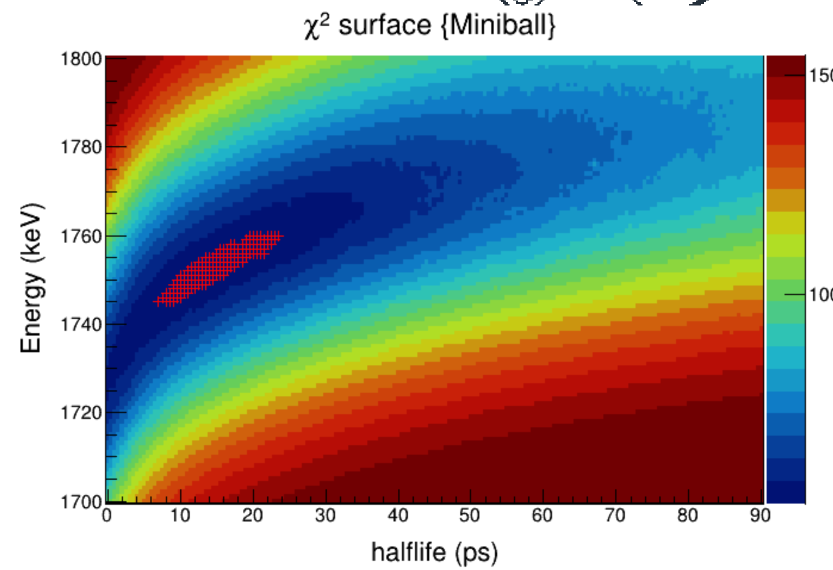

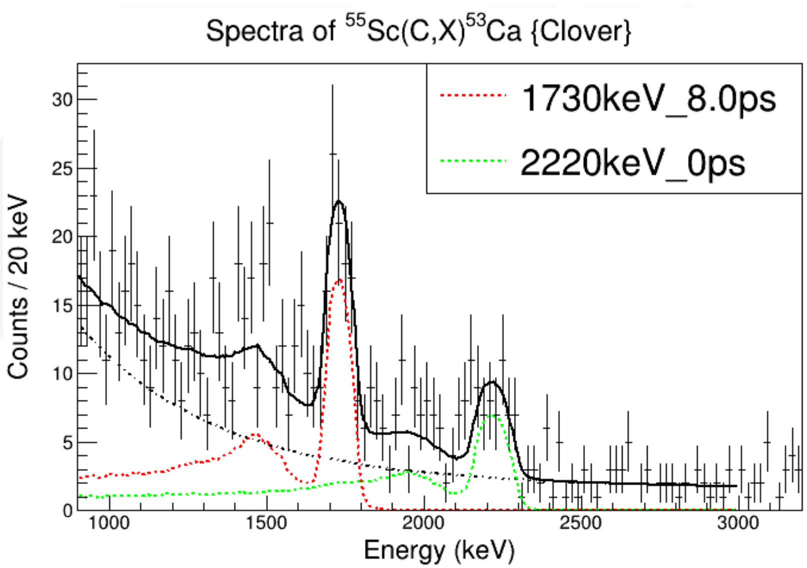

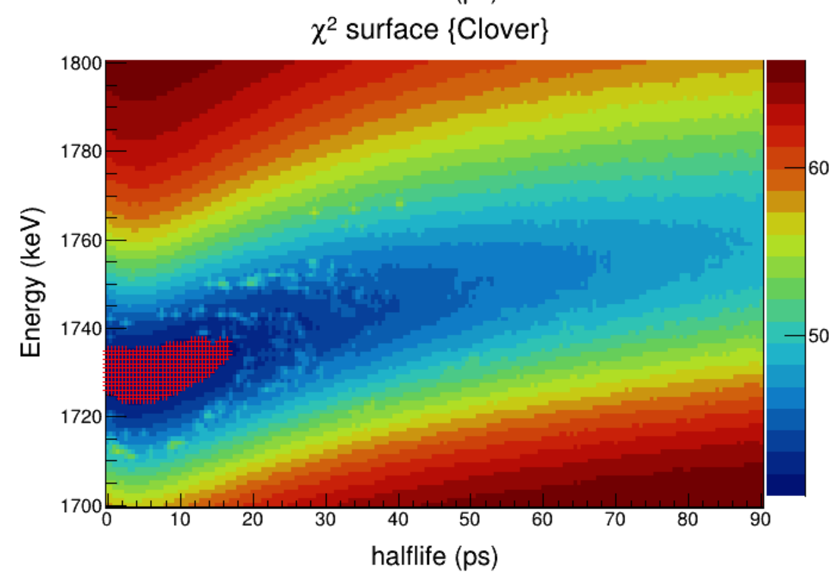

^{53}Ca from ^{55}Sc -1*p*1*n*

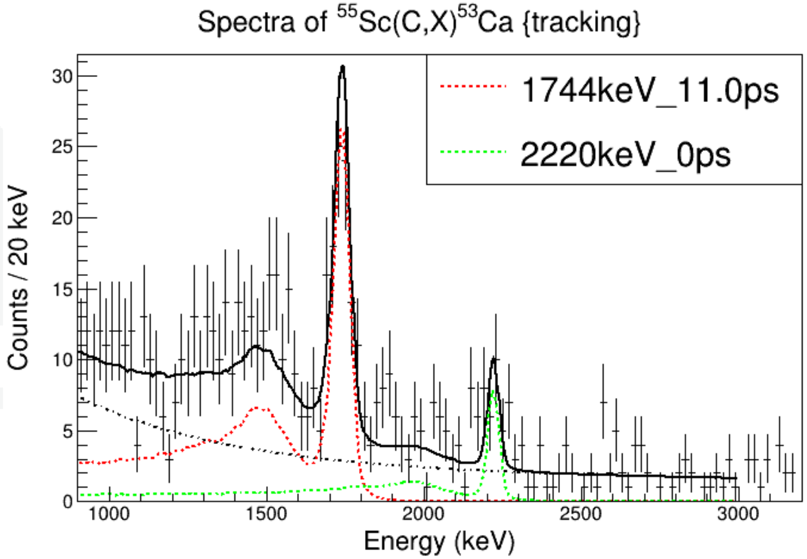

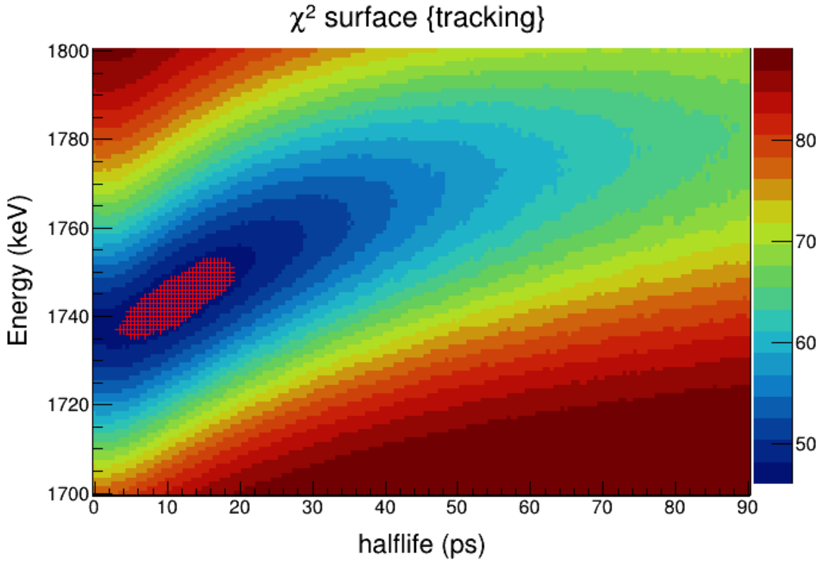

Preliminary results:

	Energy / keV	Halflife / ps
Miniball	1752(8)	15(8)
Clover	1730(6)	8(8)
tracking	1744(8)	11(8)
weighted	1740(4)	11(5)

- only statistic uncertainties are considered
- weighted by $1/\sigma^2$
- deduced $B(E2, 5/2^- \rightarrow 1/2^-) = 3.2_{-1.0}^{+2.8}\ e^2fm^4$

Theoretical calculations:

	Energy / keV	B(E2) / e^2fm^4	Halflife_E_{exp} / ps
UFP-CA	1767	5.11	7.0
VS-IMSRG	2116	0.785	45

- Shell Model calculations using UFP-CA interaction (by Alex Brown)
- Valence-space in-medium similarity renormalization group (VS-IMSRG) using chiral effective field theory (EFT) interaction (by Jason Holt, 2019)

Summary

- Performed in-beam gamma-ray spectroscopy measurement in neutron-rich Ca isotopes with a Hybrid HPGe array at RIBF
- Benchmarked the simulation with ^{36}Ar spectra, the obtained gamma-ray response functions well reproduced the peak shapes
- Analysed the ^{53}Ca spectra with detailed simulations, the lifetime of the $5/2^-$ state is extracted to be 11(5) ps, leading to a $B(E2, 5/2^- \rightarrow 1/2^-) = 3.2_{-1.0}^{+2.8}$ e^2fm^4
- Experimental results are compared with Shell-Model calculations using UFP-CA interaction, and VS-IMSRG approach using EFT interactions with 2N and 3N forces

Collaborations

University of York: S. Chen, R. Crane, W. Marshall, R. Taniuchi, M. Petri, S. Paschalis, M. Bentley, L. Tetley

RIKEN: P. Doornenbal, H. Baba, F. Browne, B. Mauss, B. Moon, H. Sakurai, D. Suzuki

RCNP: N. Aoi, E. Ideguchi, S. Iwazaki, A. Kohda, Y. Yamamoto

Universität zu Köln: C. Fransen, H. Hess, P. Reiter, S. Thiel

LBNL: H. Crawford, C. Campbell, A. Macchiavelli, P. Fallon, M. Cromaz, R. Clark, A. Frotscher

CSIC: K. Wimmer

Korea University: J. Kim

University of Tokyo: T. Koiwai

University of Surrey: T. Parry

KU Leuven: H. de Witte

TRIUMF: J. Holt

MSU: B. A. Brown

Thank you for your attention

Backup

BigRIPS Separator

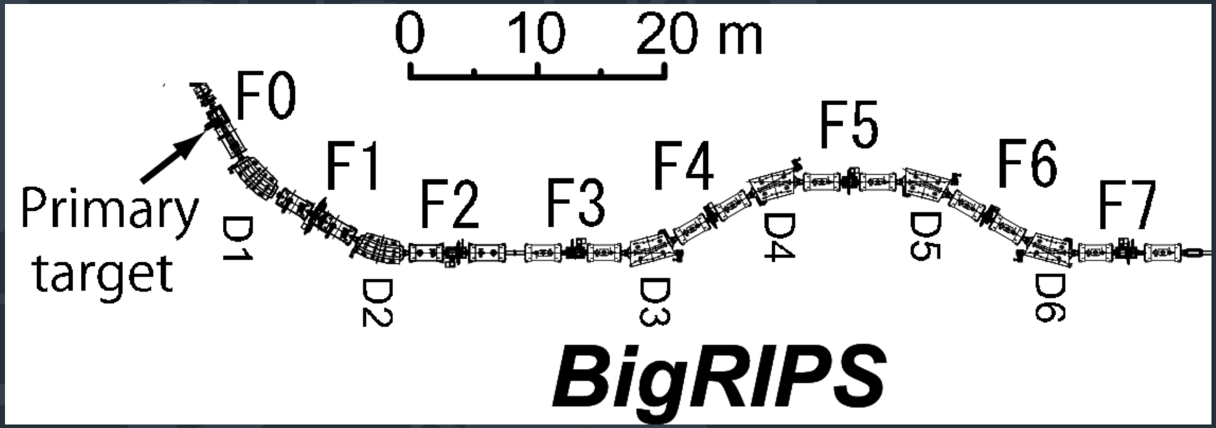

Big RIKEN Projectile Fragment Separator

- *Bρ*-Δ*E*-*Bρ* separation
- Large acceptance
  - Δ*θ* = ±40 mrad
  - Δ*φ* = ±50 mrad
  - Δp/p = ±3%
- Event-by-event *Bρ*-TOF-Δ*E* particle identification

Shell structures and nuclear forces

Woods-Saxon potential **with Spin-Orbital (L-S) force**

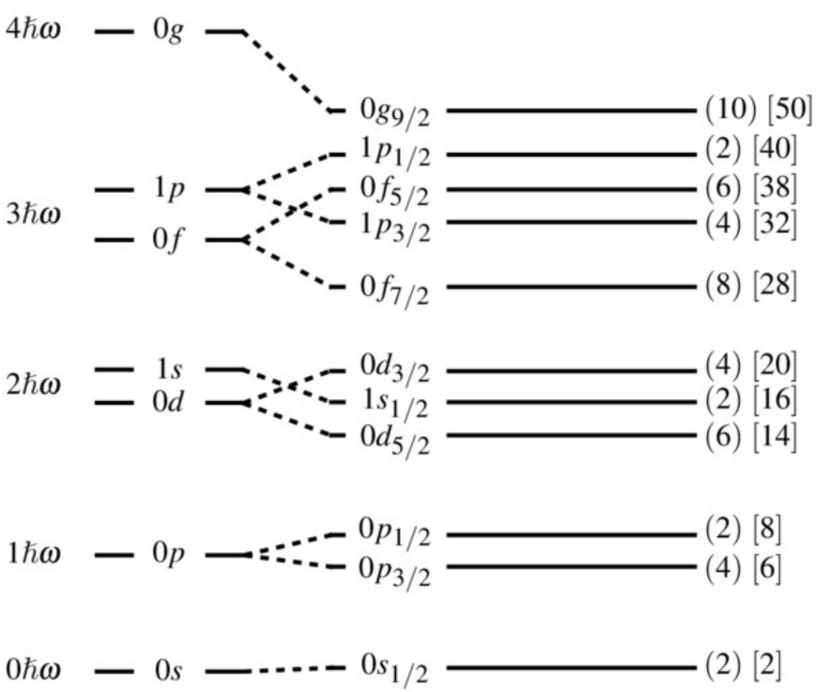

- spin-orbital splitting:
  $E(\, j_> = l + s \,) < E(\, j_< = l - s \,)$
- conventional magic numbers:
  2, 8, 20, 28, 50, ...

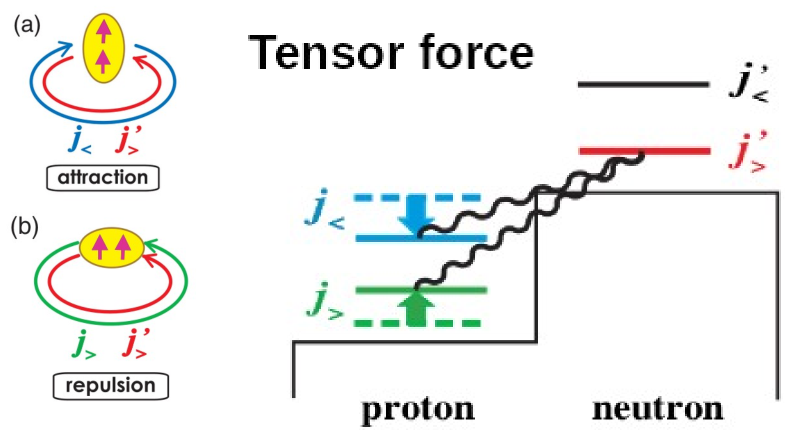

T. Otsuka *et al.*, Phys. Rev. Lett. **95**, 232502 (2005)

^{30}Si → ^{24}O: absence of strong $\pi 0d_{5/2} - \nu 0d_{3/2}$ attraction
⇒ N = 16 new magic number in oxygen

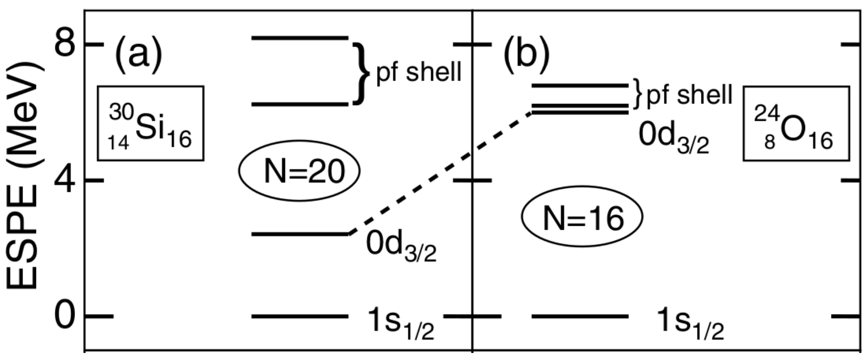

T. Otsuka *et al.*, Phys. Rev. Lett. **87**, 082502 (2001)

Shell structures and nuclear forces

Woods-Saxon potential | **with Spin-Orbital (*L*-*S*) force**

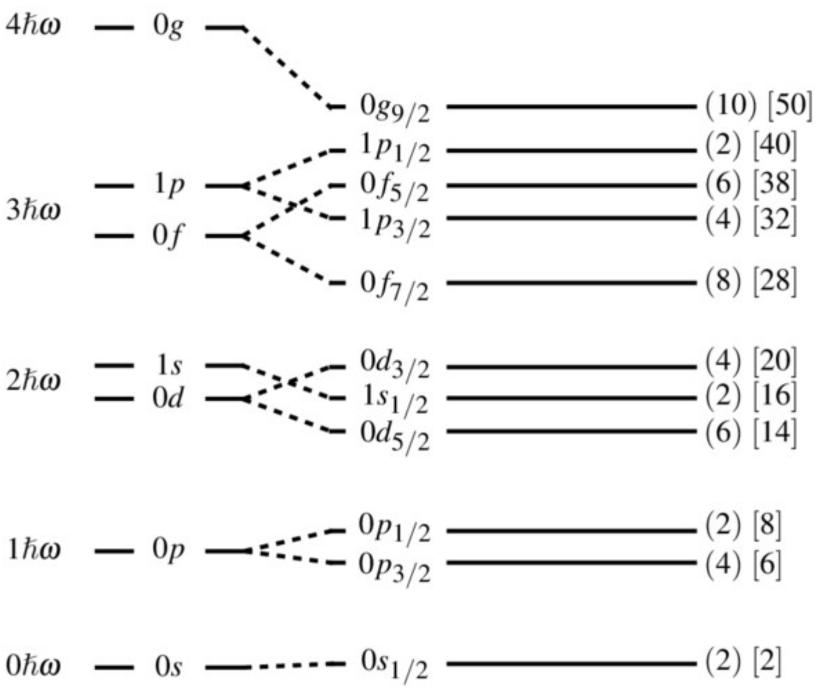

- spin-orbital splitting:
  $E(j_> = l + s) < E(j_< = l - s)$
- conventional magic numbers:
  2, 8, 20, 28, 50, ...

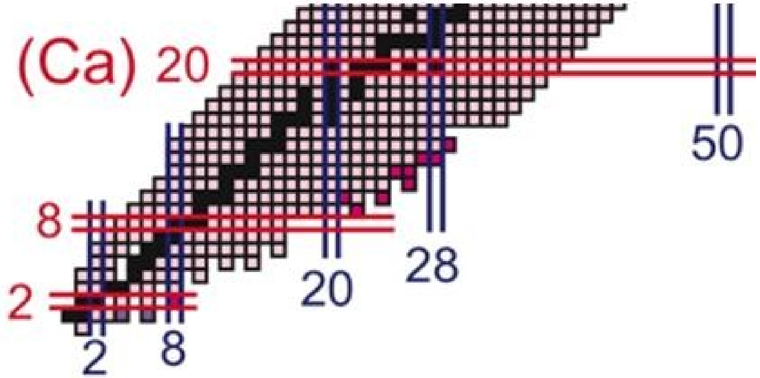

(sub-)shell closure at N = 16, 20, 28, 32, 34

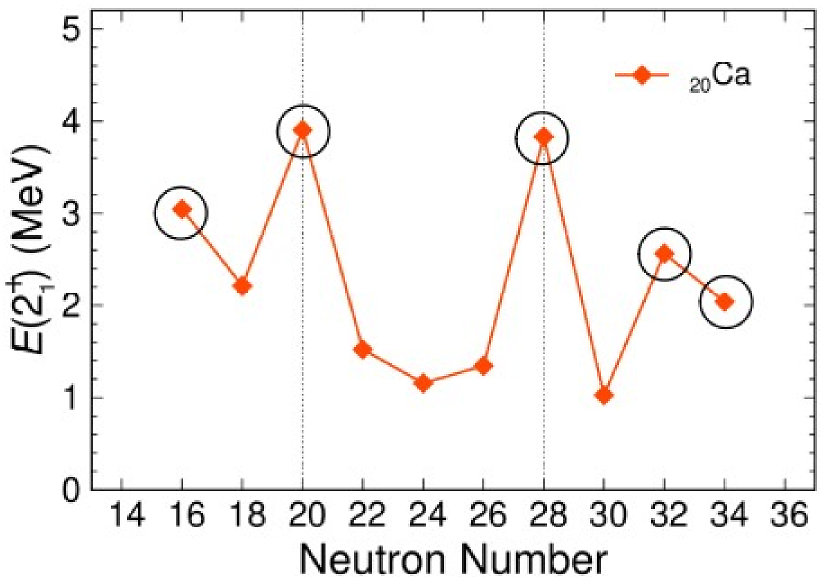

Particle Identification

neutron-rich Ca setting

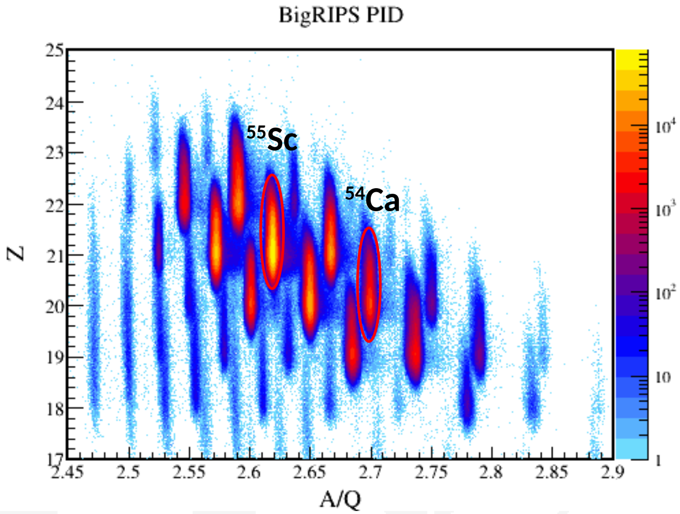

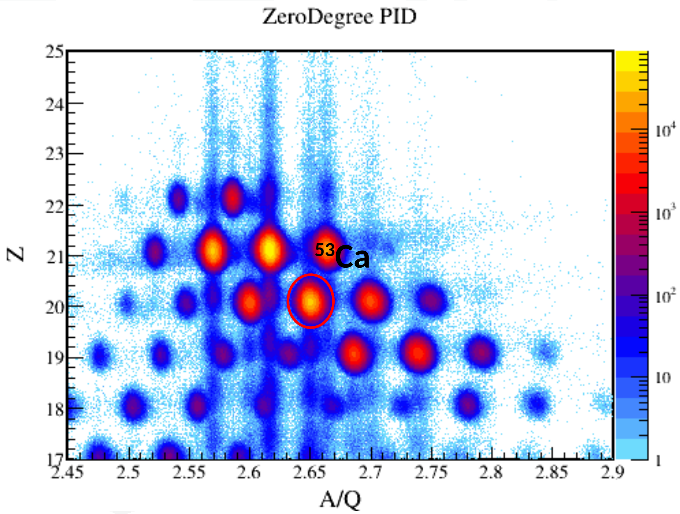

proton-rich Ca setting

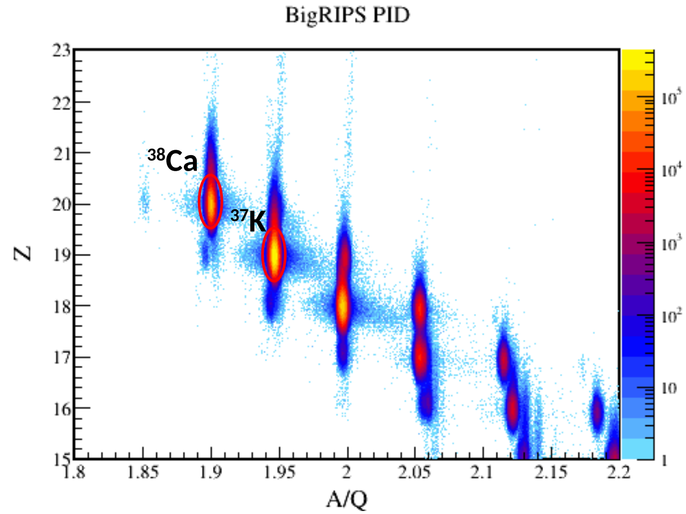

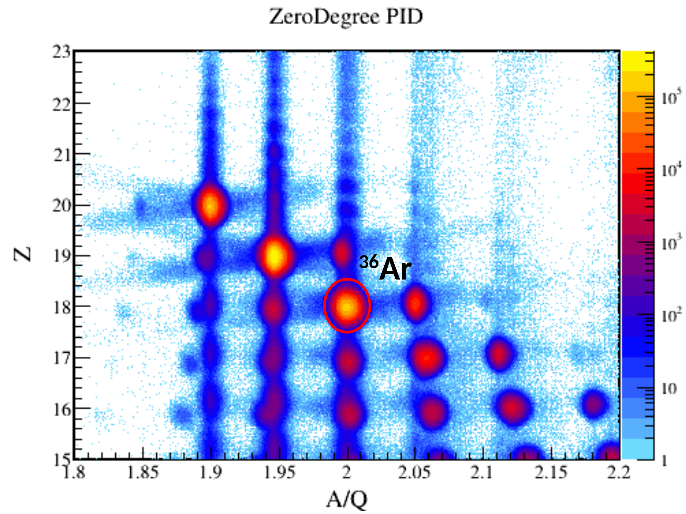

Doppler-correction

P. Doornenbal, PTEP **2012**, 03C004

- Doppler correction for prompt gamma

$$\frac{E_\gamma}{E_{\gamma 0}} = \frac{\sqrt{1-\beta^2}}{1-\beta\cos\vartheta_\gamma}$$

- Doppler-corrected gamma energy resolution:

$$\left(\frac{\Delta E_{\gamma 0}}{E_{\gamma 0}}\right)^2 = \left(\frac{\beta\sin\vartheta_\gamma}{1-\beta\cos\vartheta_\gamma}\right)^2 \times (\Delta\vartheta_\gamma)^2 + \left(\frac{\beta-\cos\vartheta_\gamma}{(1-\beta^2)(1-\beta\cos\vartheta_\gamma)}\right)^2 \times (\Delta\beta)^2 + \left(\frac{\Delta E_{\mathrm{intr}}}{E_\gamma}\right)^2.$$

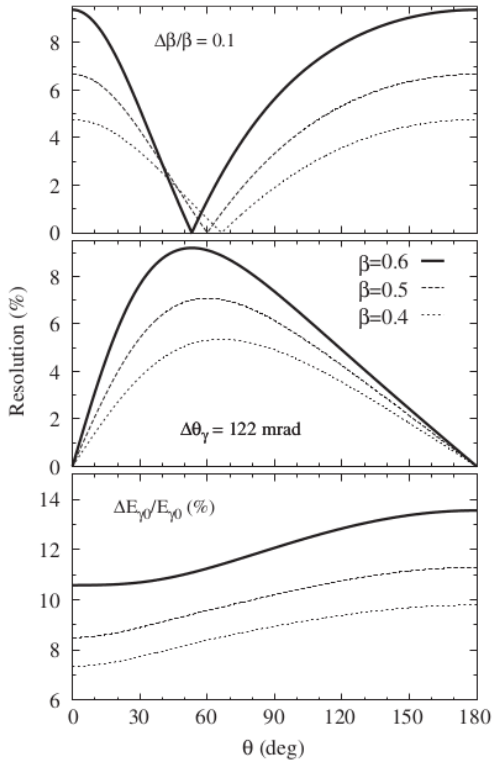

Fig. 1. Doppler broadening due to $\Delta\beta$, $\Delta\vartheta_\gamma$, and ΔE_{intr} as a function of the γ-ray emission (detector) angle ϑ_γ. Three different velocities were assumed. The upper panel displays only the velocity uncertainty effect for $\Delta\beta/\beta = 0.1$, while the middle panel displays the broadening due to a detector opening angle of $\Delta\vartheta_\gamma = 122$ mrad. In the bottom panel, the sum effect including an intrinsic energy resolution of 6% at 1.33 MeV is displayed. The calculations were performed for a 1 MeV γ-ray energy assuming a square-root dependence of the intrinsic energy resolution.

Excitation of ^{53}Ca

S. Chen *et al.*, Phys. Rev. Lett. **123**,142501 (2019)

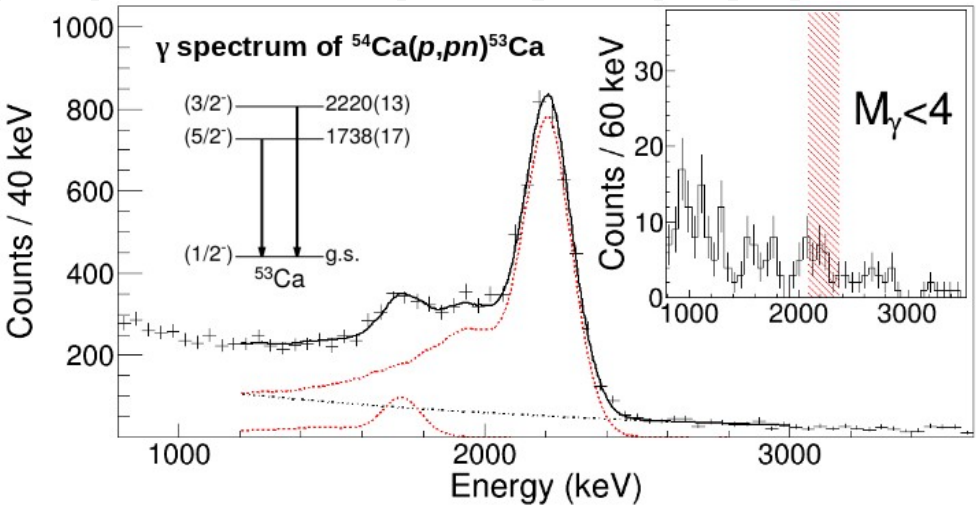

E_x = 2220 keV via β-decay,
F. Perrot *et al.* PRC **74**,014313 (2006)

^{53}Ca populated via ^{54}Ca→ ^{53}Ca

g.s. (1/2-)

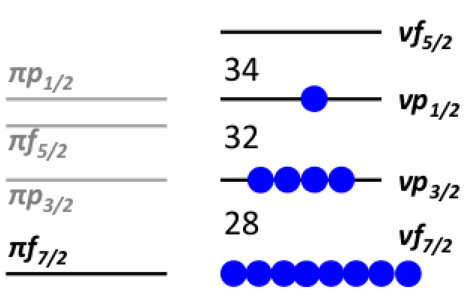

^{53}Ca (Z=20)

2220 keV (3/2-)

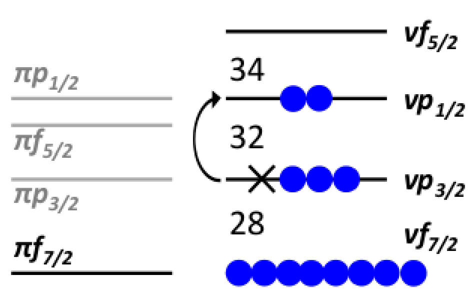

^{53}Ca (Z=20)

1753 keV (5/2-)

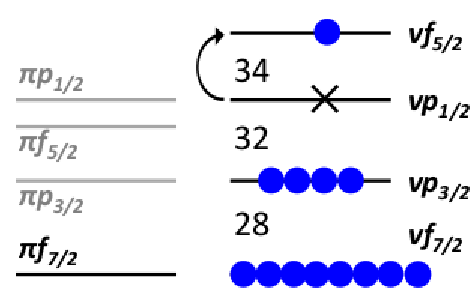

^{53}Ca (Z=20)

Benchmark – ^{36}Ar from ^{37}K -1*p*

^{36}**Ar** low-lying excitation states from NNDC

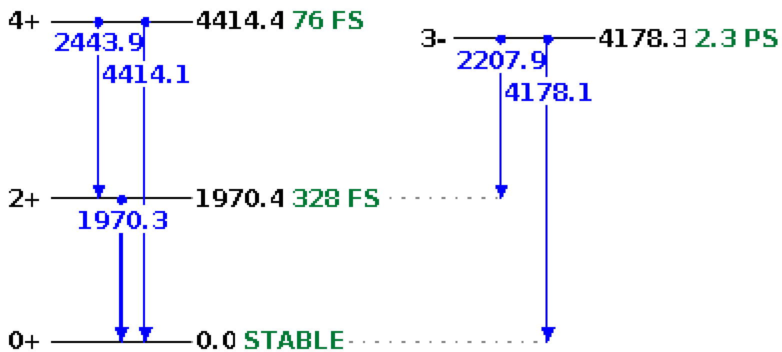

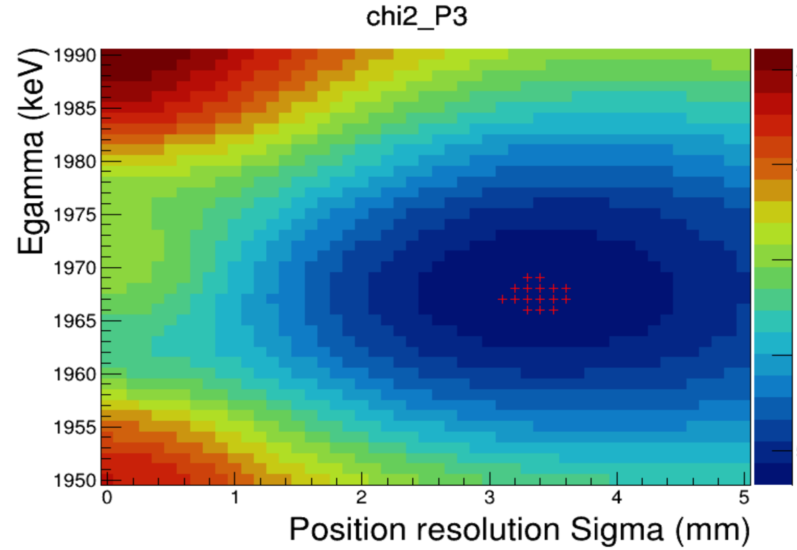

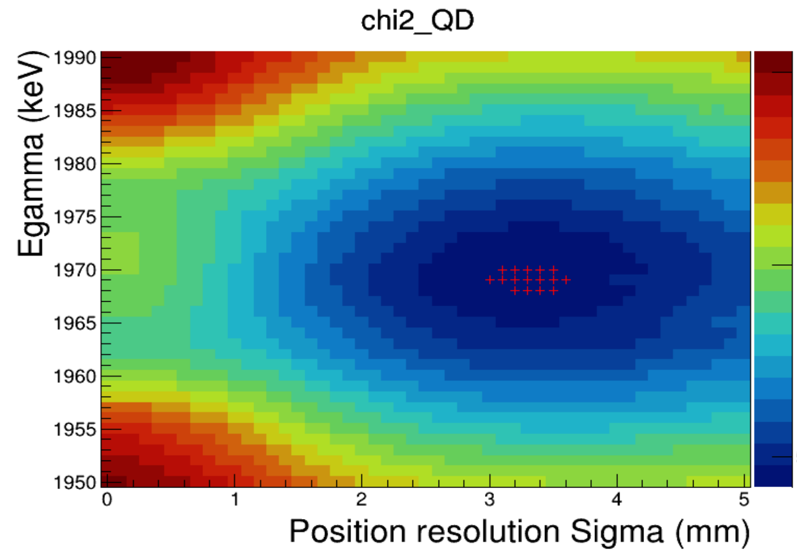

- Fix $4^+ \rightarrow 2^+$ and $3^- \rightarrow 2^+$ energies and lifetimes
- Study $2^+ \rightarrow 0^+$ energy and **tracking detectors position resolution**
- Red markers: 1-σ region (min-chi^2 +1)
- MinChi2 at

  1967keV, **3.3mm** (P3)

  1969keV, **3.3mm** (Quad)

Benchmark – ^{36}Ar from ^{37}K -1*p*

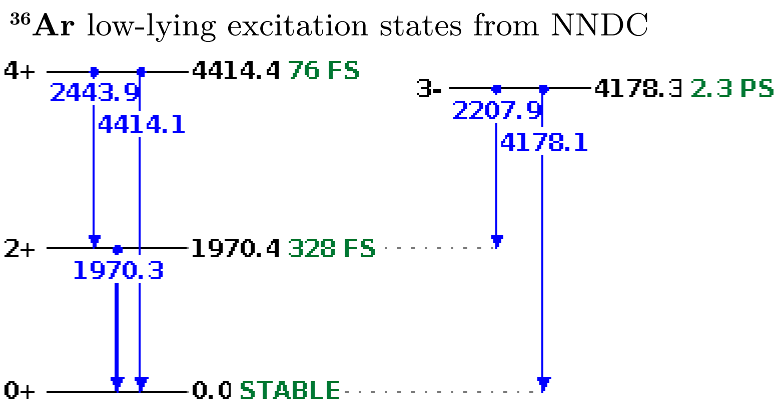

- Fix $4^+ \rightarrow 2^+$ and $3^- \rightarrow 2^+$ energies and lifetimes
- Study $2^+ \rightarrow 0^+$ energy and lifetime
- Red markers: 1-σ region (min-chi^2 +1)